รายงานวิจัยฉบับสมบูรณ์

โครงการวิจัยการประยุกต์ใช้ตัวเร่งปฏิกิริยาและเครื่องปฏิกรณ์เคมี
สำหรับใช้ในอุตสาหกรรมปิโตรเคมี
(สัญญาเลขที่ RTA4780013)

โดย ศาสตราจารย์ ดร. ปิยะสาร ประเสริฐธรรม
จุฬาลงกรณ์มหาวิทยาลัย

กรกฎาคม 2550

บทคัดย่อ

รายงานฉบับนี้สรุปผลการดำเนินงานของโครงการวิจัยการประยุกต์ใช้ตัวเร่งปฏิกิริยาและเครื่องปฏิกรณ์เคมีสำหรับใช้ในอุตสาหกรรมปิโตรเคมี ซึ่งได้รับทุนส่งเสริมกลุ่มวิจัย จากสำนักงานกองทุนสนับสนุนการวิจัย โครงการนี้นอกจากมุ่งเน้นการสร้างองค์ความรู้ใหม่ที่มีความสำคัญต่อการพัฒนาอุตสาหกรรมปิโตรเคมีแล้ว ยังเน้นการเผยแพร่ผลงานวิจัยโดยการตีพิมพ์ผลงานในวารสารระดับนานาชาติที่มีการประเมินผลงานอย่างเข้มงวด การสร้างบุคลากรที่มีความสามารถทั้งในระดับปริญญาโทและปริญญาเอก การสร้างความร่วมมือระหว่างนักวิจัยในประเทศไทยและต่างประเทศ การพัฒนาห้องปฏิบัติการวิจัยในหน่วยงานเอกชน ตลอดจนการทำวิจัยร่วมกับภาคอุตสาหกรรม

ผลที่ได้จากการดำเนินงานสามารถสรุปได้ดังนี้ คือ สามารถตีพิมพ์ผลงานในวารสารระดับนานาชาติจำนวน 42 บทความ มากกว่าเป้าหมาย 75% สามารถผลิตมหาบัณฑิตได้ 48 คน มากกว่าเป้าหมาย 60% ผลิตดุษฎีบัณฑิตได้ 13 คน มากกว่าเป้าหมาย 44% ได้สร้างความร่วมมือทางด้านงานวิจัยกับบริษัท SCG Chemical Co. Ltd. โดยสร้างห้องปฏิบัติการวิจัยเพื่อทำงานวิจัยร่วมจำนวน 1 แห่ง นอกจากนี้ ยังได้ช่วยบริษัท TUNTEX PETROCHEMICALS (THAILAND) และบริษัทระยองโอเลฟินส์ในส่วนของการเลือกตัวเร่งปฏิกิริยาที่เหมาะสมอีกด้วย ผลสำเร็จที่ได้จากโครงการฯนี้นับเป็นประโยชน์อย่างมากต่อการพัฒนาอุตสาหกรรมปิโตรเคมีของประเทศไทย

คำสำคัญ: ตัวเร่งปฏิกิริยาเคมี คาตาไลซิส นาโนคาตาไลซิส เครื่องปฏิกรณ์เคมี ปิโตรเคมี

Abstract

This report summarizes the outputs from the project entitled “Application of Catalysts and Chemical Reactors for Petrochemical Industry” under the research promotion scholarship sponsored by the Thailand Research Fund. This project was aimed to explore new basic knowledge necessary for the development of petrochemical industry. In addition, it focused on publishing the acquired knowledge in peer-review international journals, producing talent and skillful master-degree and doctoral-degree graduates, developing and strengthening the collaborations with Thai researchers and foreign professors from famous universities, promoting the establishment of a private research laboratory and developing co-research with Thai industries.

The overall outputs from the project can be summarized as follows. There are 42 international publications which are 75% higher than the expected values. The numbers of master- and doctoral-graduates are 48 and 13, higher than the expected values by 60% and 44%, respectively. The research collaboration was strongly established between our center of excellence and SCG Chemical Co. Ltd., leading to one research lab founded. In addition, the project also supported two companies; i.e., TUNTEX PETROCHEMICALS (THAILAND) and Rayong Olefins Co. Ltd, on catalyst screening. It is noted that the success from this project was very beneficial to the development of Petrochemical Industry of Thailand.

Keywords: Catalyst; Catalysis; Nanocatalysis; Chemical reactor; Petrochemical

สัญญาเลขที่ RTA4780013

รายงานวิจัยฉบับสมบูรณ์

โครงการวิจัยการประยุกต์ใช้ตัวเร่งปฏิกิริยาและเครื่องปฏิกรณ์เคมี สำหรับใช้ในอุตสาหกรรมปิโตรเคมี

โดย ศาสตราจารย์ ดร. ปิยะสาร ประเสริฐธรรม
จุฬาลงกรณ์มหาวิทยาลัย

สนับสนุนโดยสำนักงานกองทุนสนับสนุนการวิจัย

สรุปผลการดำเนินการโครงการในรอบ 3 ปี

==========

ชื่อหัวหน้าโครงการ ศ.ดร. ปิยะสาร ประเสริฐธรรม

รายงานในช่วงเวลาตั้งแต่วันที่ 1 สิงหาคม พ.ศ. 2547 **ถึง** 31 กรกฎาคม พ.ศ. 2550

1. กิจกรรมที่ได้ดำเนินการ

1.1 ด้านการประสานงานระหว่างผู้ดำเนินการ

เนื่องจากคณะผู้วิจัยประกอบด้วยอาจารย์และนักวิจัยจากหลายสถาบัน การติดต่อประสานงานจึงดำเนินการด้วยวิธีดังนี้

1. รศ.ดร. ชาคริต ทองอุไร (มหาวิทยาลัยสงขลานครินทร์)
   การติดต่อทำโดยการโทรศัพท์
2. อ.ดร.ชูวงศ์ ชัยสุข (มหาวิทยาลัยศิลปากร)
   การติดต่อทำโดยการโทรศัพท์และเดินทางเข้ามาที่ภาควิชาวิศวกรรมเคมี คณะวิศวกรรมศาสตร์ จุฬาลงกรณ์มหาวิทยาลัย ประมาณสัปดาห์ละครั้ง
3. อ.ดร. โอกร เมฆาสุวรรณดำรง (มหาวิทยาลัยศิลปากร)
   การติดต่อทำโดยการโทรศัพท์และเดินทางเข้ามาที่ภาควิชาวิศวกรรมเคมี คณะวิศวกรรมศาสตร์ จุฬาลงกรณ์มหาวิทยาลัย ประมาณสัปดาห์ละครั้ง
4. ดร. นครินทร์ มงคลศิริ (บริษัทระยองโอเลฟินส์ จำกัด)
   การติดต่อทำโดยการโทรศัพท์และเดินทางเข้ามาที่ภาควิชาวิศวกรรมเคมี คณะวิศวกรรมศาสตร์ จุฬาลงกรณ์มหาวิทยาลัย ประมาณเดือนละครั้ง
   นอกจากนี้ ดร.จูงใจ ปั้นประณต เดินทางไปที่โรงงานประมาณ 3 เดือนครั้ง

2. ผลงาน

2.1 บทความวิจัยในวารสารระดับนานาชาติ

2.1.1 บทความที่ได้รับการตอบรับแล้ว จำนวน 42 ผลงาน

1. S. Sombatchaisak, P. P. Praserthdam, C. Chaisuk and J. Panpranot, “An Alternative Correlation Equation between Particle Size and Structure Stability of H-Y Zeolite under Hydrothermal Treatment Condition”, Ind. Eng. Chem. Res. 43 (2004) 4066-4072. (Impact factor 2004 = 1.424) (เอกสารแนบชุดที่ 1)
2. W. Sangtongkitcharoen, S. Assabumrungrat, V. Pavarajarn, N. Laosiripojana, and P. Praserthdam, “Comparison of Carbon Formation Boundary for Different Types of Solid Oxide Fuel Cells with Methane Feed”, J. Power Sources, 142 (1-2) , 75-80

(2005) (Impact factor 2005 = 2.770). (เอกสารแนบชุดที่ 2)

3. B. Jongsomjit, C. Sakdamnuson, and P. Praserthdam, “Dependence of crystalline phases in titania on catalytic properties during CO hydrogenation of Co/TiO_2 catalysts”, Materials Chemistry and Physics 89 (2005) 395-401. (Impact Factor 2005 = 1.136) (เอกสารแนบชุดที่ 3)
4. B. Jongsomjit, E. Chaichana and P. Praserthdam, “LLDPE/nano-silica composites synthesized via in situ polymerization of ethylene-1-hexene with MAO/metallocene catalyst” Journal of Materials Science 40 (8), 2043-2045 (2005) (Impact factor 2005 = 0.901). (เอกสารแนบชุดที่ 4)
5. B. Jongsomjit, T. Wongsalee and P. Praserthdam, “Study of Cobalt Dispersion on Titania Consisting Various Rutile Anatase Ratios” Materials Chemistry and Physics 92 (2-3), 572-577. (2005) (Impact factor 2005 = 1.136). (เอกสารแนบชุดที่ 5)
6. B. Jonsomjit**,** S. Ngamposri, and P. Praserthdam, “Catalytic activity during copolymerization of ethylene/1-hexene via mixed TiO_2/SiO_2-supported MAO with rac-Et$[Ind]_2ZrCl_2$ metallocene catalyst”, Molecules, (2005), 10, 603-609 (Impact factor 2005 = 1.113) (เอกสารแนบชุดที่ 6)
7. P. Praserthdam, C. Chaisuk, W. Kongsuebchart, S. Thongyai, S.K.N. Ayudhya, New concepts in material and energy utilization, Korean Journal of Chemical Engineering 22 (1) , 115-120 (2005) (Impact factor 2005 = 0.750) (เอกสารแนบชุดที่ 7)
8. B. Jongsomjit, S. Ngamposri, and P. Praserthdam, “Role of titania in TiO_2-SiO_2 mixed oxides-supported metallocene catalyst during ethylene/1-octene copolymerization”, Catalysis Letters, 100 (3-4) 139 – 146 (2005) (Impact factor 2005 = 2.088) (เอกสารแนบชุดที่ 8)
9. J. Panpranot, S. Kaewgun, and P. Praserthdam, “Metal-Support Interaction in Mesoporous Silica Supported Cobalt Fischer-Tropsch Catalysts”, Reaction Kinetics and Catalysis Letters, 85, (2005) 299-304. (Impact factor 2005 = 0.670) (เอกสารแนบชุดที่ 9)
10. P. Soisuwan, P. Praserthdam, Dean C. Chambers, David L. Trimm, O. Mekasuwandumrong, and J. Panpranot, “Characteristics and Catalytic Properties of Alumina-Zirconia Mixed Oxides Prepared by the Modified Pechini Method”, Catalysis Letters, 103 (2005) 63-68. (Impact factor 2005 = 2.088) (เอกสารแนบที่ชุดที่ 10)
11. B. Jongsomjit, A. Khotdee, and P. Praserthdam, “Behaviors of ethylene/norbornene

copolymerization with zirconocene catalysts", Iranian Polymer Journal, 14, 559 - 564 (2005). (Impact factor 2005 = 0.316) (เอกสารแนบชุดที่ 11)

12. S. Assabumrungrat, W. Sangtongkitcharoen, N. Laosiripojana, A. Arpornwichanop, Sumittra Charojrochkul and P. Praserthdam, "Effects of Electrolyte Type and Flow Pattern Mode on Performances of Methanol-Fueled Solid Oxide Fuel Cells" J. Power Sources 148 (2005) 18-23 (Impact factor 2005 = 2.770) (เอกสารแนบชุดที่ 12)
13. J. Panpranot, L. Nakkararuang, B. Ngamsom and P. Praserthdam, "Synthesis, Characterization, and Catalytic Properties of Pd and Pd-Ag Catalysts Supported on Nanocrystalline TiO_2 Prepared by the Solvothermal Method", Catalysis Letters, 103 (2005) 53-58. (Impact factor 2005 = 2.088) (เอกสารแนบที่ชุดที่ 13)
14. J. Panpranot, K. Pattamakomsan, and P. Praserthdam, "Deactivation of Silica Supported Pd Catalysts during Liquid-Phase Hydrogenation" Reaction Kinetics and Catalysis Letters, 86 (2005) 141-147. (Impact factor 2005 = 0.670) (เอกสารแนบชุดที่ 14)
15. J. Panpranot, **K.** Toophorm, and P. Praserthdam, "Effect of Particle Size on the Hydrothermal Stability and Catalytic Activity of Polycrystalline Beta Zeolite" Journal of Porous Materials, 12 (2005) 301-307 (Impact factor 2005 = 0.698) (เอกสารแนบชุดที่ 15)
16. J. Panpranot, N. Taochaiyaphum, and P. Praserthdam, "Glycothermal Synthesis of Nanocrystalline Zirconia and their Applications as Cobalt Catalyst Supports" Materials Chemistry and Physics, 94 (2005) 207-212 (Impact factor 2005 = 1.136) (เอกสารแนบชุดที่ 16)
17. B. Jongsomjit, S. Phoowakeereewiwat, S. Thongyai, T. Shiono, and P. Praserthdam, "Impact of diene addition on properties for ethylene-propylene copolymerization with rac-Et[Ind]$_2$$ZrCl_2$/MAO catalyst", Materials Letters, 59, 3771 – 3774 (2005) (Impact factor 2005 = 1.299) (เอกสารแนบชุดที่ 17)
18. B. Jongsomjit, T. Wongsalee, and P. Praserthdam, "Characteristics and catalytic properties of Co/TiO_2 for various rutile:anatase ratios", Catalysis Communications, 6, 705 – 710 (2005) (Impact factor 2005 = 2.098) (เอกสารแนบชุดที่ 18)
19. Joongjai Panpranot, Nuttakarn Taochaiyaphum, Bunjerd Jongsomjit, and Piyasan Praserthdam "Differences in Characteristics and Catalytic Properties of Co Catalysts Supported on Micron- and Nano-Sized Zirconia" Catalysis Communications 7 (2006) 192-197. (Impact factor 2005 = 2.098) (เอกสารแนบชุดที่

19)

20. J. Klongdee, W. Petchkroh, K. Phuempoonsathaporn, P. Prasertdam, A.S. Vangnai, and V. Pavarajarn, "Activity of Nanosized Titania Synthesized from Thermal Decomposition of Titanium (IV) n-Butoxide for the Photocatalytic Degradation of Diuron", Science and Technology of Advanced Materials, 6 (3-4 SPEC. ISS.), 290-295. (Impact factor 2005 = -) (เอกสารแนบชุดที่ 20)
21. B. Jongsomjit, T. Wongsalee, and P. Praserthdam, "Catalytic behaviors of mixed TiO_2-SiO_2-supported cobalt Fischer-Tropsch catalysts for carbon monoxide hydrogenation", Materials Chemistry and Physics 97 (2006) 343-350 (Impact factor 2005 = 1.136) (เอกสารแนบชุดที่ 21)
22. T. Wongsalee, B. Jongsomjit and P. Praserthdam, "Effect of Zirconia-Modified Titania Consisting of Different Phases on Characteristics and Catalytic Properties of Co/TiO_2 Catalysts", Catalysis Letters 108 (2006) 55-61 (Impact factor 2005 = 2.088) (เอกสารแนบชุดที่ 22)
23. Joongjai Panpranot, Nuttakarn Taochaiyaphum, and Piyasan Praserthdam "Effect of Si Addition on the Properties of Nanocrystalline ZrO_2-Supported Cobalt Catalysts" Reaction Kinetics and Catalysis Letters 87 (2006) 185-190. (Impact factor 2005 = 0.670) (เอกสารแนบชุดที่ 23)
24. Patta Soisuwan, Joongjai Panpranot, David L. Trimm and Piyasan Praserthdam "A Study of Alumina-Zirconia Mixed Oxides Prepared by the Modified Pechini Method as Co Catalyst Supports in CO Hydrogenation" Applied Catalysis A. General 303 (2006) 268-272. (Impact factor 2005 = 2.728) (เอกสารแนบชุดที่ 24)
25. Patta Soisuwan, Piyasan Praserthdam, Joongjai Panpranot, and David L. Trimm "Effects of Si- and Y-Modified Nanocrystalline Zirconia on the Properties of Co/ZrO_2 Catalysts" Catalysis Communications 7 (2006) 761-767 (Impact factor 2005 = 2.098) (เอกสารแนบชุดที่ 25)
26. Bunjerd Jongsomjit, Chitlada Sakdamnuson, Joongjai Panpranot, and Piyasan Praserthdam "Roles of ruthenium on reduction behaviors of ruthenium-promoted cobalt/titania Fischer-Tropsch catalyst", Reaction Kinetics and Catalysis Letters, 88 (2006), 65-71 (Impact factor 2005 = 0.670). (เอกสารแนบชุดที่ 26)
27. Bunjerd Jongsomjit, Tipnapa Wongsalee, and Piyasan Praserthdam "Elucidation of reduction behaviors for Co/TiO_2 catalysts with various rutile/anatase ratios", Studies

in Surface Science and Catalysis, 159 (2006), 285-288. (Impact factor 2005 = 0.307). (เอกสารแนบชุดที่ 27)

28. Watcharapong Khaodee, Bunjerd Jongsomjit, Suttichai Assabumrungrat, Piyasan Praserthdam, and Shigeo Goto, "Investigation of isosynthesis via CO hydrogenation over ZrO_2 and CeO_2 catalysts: effects of crystallite size, phase composition and acid-base sites" Catalysis communications 8 (2007) 548-556 (Impact factor 2005 = 2.098). (เอกสารแนบชุดที่ 28)
29. Joongjai Panpranot, Kunyaluck Kontapakdee, and Piyasan Praserthdam "Selective Hydrogenation of Acetylene in Excess Ethylene on Micron-Sized and Nanocrystalline TiO_2 Supported Pd Catalysts" *Applied Catalysis A: General* 314 (2006) 128-133 (Impact factor 2005 = 2.728). (เอกสารแนบชุดที่ 29)
30. Wilasinee Kongsuebchart, Piyasan Praserthdam, Joongjai Panpranot, Akawat Sirisuk, Piyawat Supphasrirongjaroen, and Chairit Satayaprasert "Effect of Crystallite Size on the Surface Defect of Nano-TiO_2 Prepared via Solvothermal Synthesis" *Journal of Crystal Growth* 297 (2006) 234-238 (Impact factor 2005 = 1.681). (เอกสารแนบชุดที่ 30)
31. Jongsomjit, B., Sakdamnuson, C., Panpranot, J., Praserthdam, P., "Role of ruthenium in the reduction behavior of ruthenium-promoted cobalt/titania Fischer-Tropsch catalysts", Reaction Kinetics and Catalysis Letters 88 (2006) 65-71 (Impact factor 2005 = 0.670). (เอกสารแนบชุดที่ 31)
32. Jongsomjit, B., Wongsalee, T., Praserthdam, P., "Elucidation of reduction behaviors for Co/TiO2 catalysts with various rutile/anatase ratios", Studies Surface Science and Catalysis 159 (2006) 285-288 (Impact factor 2005 = 0.307). (เอกสารแนบชุดที่ 32)
33. Chaichana, E., Jongsomjit, B., Praserthdam, P., "Effect of nano-SiO2 particle size on the formation of LLDPE/SiO2 nanocomposite synthesized via the in situ polymerization with metallocene catalyst", Chemical Engineering Science 62 (2006) 899-905 (Impact factor 2005 = 1.735). (เอกสารแนบชุดที่ 33)
34. Okorn Mekasuwandumrong, Varong Pavarajarn, Masashi Inoue and Piyasan Praserthdam, "Preparation and phase transformation behavior of χ-alumina via solvothermal synthesis", Materials Chemistry and Physics 100 (2006) 445-450 (Impact factor 2005 = 1.136). (เอกสารแนบชุดที่ 34)

35. Chalermpol Wonglert, Supakanok Thongyai, Piyasan Praserthdam, “Effect of Aging on Synthesis of Graft Copolymer of EPDM and Styrene”, J. Applied Polymer Science, **102 (5), pp. 4809-4813** (**Impact factor** 2005 = 1.072). **(เอกสารแนบชุดที่ 35)**
36. Satit Thanyaprueksanon, Supakanok Thongyai, Piyasan Praserthdam, “New synthesis method for polypropylene co ethylene-propylene rubber”, J. Applied Polymer Science, **103 (6), pp. 3609-3616** (**Impact factor** 2005 = 1.072). **(เอกสารแนบชุดที่ 36)**
37. Lerdlaksana Ubonnut, Supakanok Thongyai, Piyasan Praserthdam“ Interfacial adhesion enhancement of polyethylene-polypropylene mixture”, J. Applied Polymer Science, **104 (6), pp. 3766-3773** (**Impact factor** 2005 = 1.072). **(เอกสารแนบชุดที่ 37)**
38. Bunjerd Jongsomjit, Joongjai Panpranot, and Piyasan Praserthdam “Effect of nanoscale SiO_2 and ZrO_2 as the fillers on the microstructure of LLDPE nanocomposites synthesized via in situ polymerization with zirconocene”, Materials Letters, 61 (2007) 1376-1379 (Impact factor 2005 = 1.299). **(เอกสารแนบชุดที่ 38)**
39. Kamonchanok Pansanga, Okorn Mekasuwandumrong, Joongjai Panpranot, and Piyasan Praserthdam “Synthesis of Nanocrystalline Al_2O_3 by Thermal Decomposition of Aluminum Isopropoxide and its Application as Co Catalyst Support for Carbon Monoxide Hydrogenation” Korean Journal of Chemical Engineering, in press (**Impact factor** 2005 = 0.750).
40. Sujittra Kittiruangrayab, Tanuchnun Burakorn, Bunjerd Jongsomjit, and Piyasan Praserthdam, ”Characterization of cobalt dispersed on various micro- and nanoscale silica and zirconia supports”, Catalysis Letters, in press (**Impact factor** 2005 = 2.088).
41. **Parawee Tonto, Okorn Mekasuwandumrong, Suphot Phatanasri, Varong Pavarajarn and Piyasan Praserthdam, “Preparation of ZnO nanorod by solvothermal reaction of zinc acetate in various alcohols”, Ceramics International, in press (Impact factor 2005 = 0.702).**
42. **Kamonchanok Pansanga, Joongjai Panpranot, Okorn Mekasuwandumrong, Chairit Satayaprasert, and Piyasan Praserthdam “Effect of Mixed γ and χ Crystalline**

Phases in Nanocrystalline Al_2O_3 on the Dispersion of Cobalt on Al_2O_3" Catalysis Communications, accepted June 2007 (Impact factor 2005 = 2.098).

2.1.2 บทความที่อยู่ระหว่างการแก้ไข จำนวน 2 ผลงาน

1. Piyawat Supphasrirongjaroen, Piyasan Praserthdam, Joongjai Panpranot, and Duangkamol Na-Ranong "Effect of Quenching Medium on Photocatalytic Activity of Nano-Sized TiO_2 Prepared by Solvothermal Method" Chemical Engineering Journal, Submitted Revised Manuscript.
2. Kamonchanok Pansanga, Nattaporn Lohitharn, Andrew C. Y. Chien, Edgar Lotero, Joongjai Panpranot, Piyasan Praserthdam, and James G. Goodwin, Jr. "Copper-Modified Alumina as a Support for Iron Fischer Tropsch Synthesis Catalysts" *Applied Catalysis A. General*, June (2007). Submitted Revised Manuscript.

2.2 ผู้สำเร็จการศึกษาระดับปริญญาเอก จำนวน 5 คน

1. นายวรพล เกียรติกิตติพงษ์
2. น.ส.พัทธา สร้อยสุวรรณ
3. นายนวพร อินทรกำจร
4. น.ส.กมลชนก ปานสง่า
5. นายก้องเกียรติ สุริเย

หมายเหตุ นิสิตระดับปริญญาเอก อีกจำนวน 4 คน กำลังจะสำเร็จการศึกษา ดังรายชื่อต่อไปนี้

1. นายการุณย์ ธนรังสรรค์ จะสอบวิทยานิพนธ์ ในเดือนกันยายน 2550
2. น.ส.วิลาสินี คงสืบชาติ จะสอบวิทยานิพนธ์ ในเดือนกันยายน 2550
3. น.ส.วาสนา แจ่มศักดิ์ จะสอบวิทยานิพนธ์ ในเดือนมีนาคม 2551
4. น.ส.ศิรชญา กุญชร ณ อยุธยา จะสอบวิทยานิพนธ์ ในเดือนมีนาคม 2551
5. นายกิตติ ตั้งจิตเอื้อบุญ จะสอบวิทยานิพนธ์ ในเดือนมีนาคม 2551
6. นายฉัตรชัย มีโภคา (เต้) จะสอบวิทยานิพนธ์ ในเดือนมีนาคม 2551
7. นายสถาพร คำหอม (ยุ้ย) จะสอบวิทยานิพนธ์ ในเดือนมีนาคม 2551
8 นายปิยะวัฒน์ ศุภศรีรุ่งเจริญ จะสอบวิทยานิพนธ์ ในเดือนมีนาคม 2551

2.3 ผู้สำเร็จการศึกษาระดับปริญญาโท จำนวน 48 คน

1. นายสุทธิ งามโพธิศรี
2. น.ส.ศิริพร ไพศาลสิงห์
3. น.ส. จันทรา วิวัฒนพงษ์พันธ์
4. น.ส.ปารวี โทนโต๊ะ

5. น.ส.อรทัย ตั้งจิตวัฒนาการ
6. น.ส.ฤทัยรัตน์ ปรีชายุทธศิลป์
7. นายพิเชษฐ์ พหุพงศ์ทรัพย์
8. น.ส.อำไพพรรณ ศิวะวิชชกิจ
9. น.ส.รัชฎาภรณ์ นิลเพชร
10. นายจีรพงษ์ วัฒนาอรุณ
11. น.ส.อมรรัตน์ เหมือนภักตร์
12. น.ส.เกศสุดา ชัยรัตน์
13. น.ส.ลักขณา นครเรือง
14. น.ส.ณัฐกานต์ เต้าชัยภูมิ
15. นายอุกฤษ์ สหพัฒนสมบัติ
16. น.ส.คณิตา ธรรมะจริยวงศา
17. น.ส.ธนิษฐา ประสิทธิวุฒิศักดิ์
18. น.ส. ทิพย์นภา วงค์สลี
19. นายเอกราชันย์ ไชยชนะ
20. น.ส.สิรีธร ภูวคีรีวิวัฒน์
21. น.ส.อรกนก บุญธรรมติระวุฒิ
22. นายสนธิ ขำสว่าง
23. น.ส.ณฐินี ศรีเนตร
24. นายรุ่งโรจน์ ชาญชัยฤกษ์
25. น.ส.สุรีย์พร ศักดิ์ภาวุฒิ
26. นายสืบสกุล โพธิ์เกษม
27. นายทรงพล อังคพิพัฒนชัย
28. น.ส.ดรุณี สุขหอม
29. นายวัชรพงษ์ ขาวดี
30. นายวิบูลย์ แสงทองกิจเจริญ
31. น.ส.กรรณิการ์ แผ่นดินทอง
32. นายเอกวุฒิ ภูมิพิเชฐ
33. นายศุภวุฒิ ภู่ภัทรกุล
34. นายธนัชนันนท์ บูรกรณ์
35. นายขวัญพงศ์ เหมือนโพธิ์
36. นายพีรพล บัวแก้ว

37. น.ส.เลิศลักษณา อุบลนุช
38. นายเอกพล พรหมรส
39. น.ส.นิธิพร แสงเงิน
40. น.ส.รัตนวลี ศูนย์พลอย
41. นายประพัฒน์ ทนงคงสวัสดิ์
42. นายพิชิต ทิศทวีรัตน์
43. น.ส.เบญจพร เมืองสมบัติ
44. นายวรุณ วิมลสถิตย์
45. น.ส.ปวีณา เดือนฉาย
46. น.ส.กัลญาลักษณ์ คนธภักดี
47. น.ส.สุจิตรา กิตติเรืองระยับ
48. นายสาธิต ธัญญพฤกษานนท์

3. กิจกรรมอื่น ๆ ที่เกี่ยวข้อง

3.1 การนำเสนอผลงานในที่ประชุมระดับนานาชาติ

3.1.1 The 13th International Congress on Catalysis, July 11-15, (2004) Paris, France.

1. J. Panpranot, S. Kaewgun, and P. Praserthdam “Metal-Support Interaction in Mesoporous Silica Supported Cobalt Fischer-Tropsch Catalysts”.

3.1.2 Regional Symposium on Chemical Engineering (RSCE 2004), Bangkok, December 1 – 3, 2004

1. W. Sangtongkitcharoen, S. Assabumrungrat, V. Pavarajarn, N. Laosiripojana and P. Praserthdam “Prediction of Boundary of Carbon Formation for Different Types of Solid Oxide Fuel Cells with Methane Feed”.
2. N. Taochaiyapoom, J. Panpranot, and P. Praserthdam “Characteristics of Cobalt Catalysts Supported on Zirconia Nanoparticles Prepared by Glycothermal Method”.
3. O. Tungjitwattakarn, J. Panpranot, and P. Praserthdam “Liquid Phase Hydrogenation on Silica Supported Pd Catalysts: Effects of Pd Precursors and Reduction Temperature”.
4. L. Nakkararuang, J. Panpranot, B. Ngamsom, and P. Praserthdam "Selective hydrogenation of acetylene on Pd catalysts supported on solvothermal-derived TiO_2”.

5. S. Ngamposri S, B. Jongsomjit, and P. Praserthdam, “Ethylene/1-octene copolymerization using mixed titania/silica-supported MAO with zirconocene catalyst”.
6. E. Chaichana, B. Jongsomjit, and P. Praserthdam, “Synthesis of LLDPE/silica-nanocomposites by in situ polymerization with MAO/zirconocene catalyst”.
7. T. Wongsalee, B. Jongsomjit, and Praserthdam P., “Dependence of crystalline forms of titania on catalytic properties of Co/TiO_2 catalysts”.
8. C.Wonglert, S.Thongyai, P.Praserthdam, “Blend Properties and Synthesis of Graft-copolymer between Ethylene-Propylene-Diene Terpolymer and Styrene”.
9. E.Singnoo, S.Thongyai, P.Praserthdam, “Effects of Low Molar Mass Liquid Crystal and Lubricant Additive on the Crystallinity of Isotactic Polypropylene”.
10. A.Buasri, S.Thongyai, P.Praserthdam, “Effects of Low Molar Mass Liquid Crystal and Lubricant Additive on the Crystallinity of Syndiotactic Polystyrene”.
11. J.Klongdee, V.Pavarajarn, O.Mekasuwandumrong and P.Praserthdam, “Photocatalytic Degradation of Methylene Blue by TiO_2 Nanocrystals Synthesized via Thermal Decomposition of Titanium (IV) n-Butoxide in Organic Solvents”.
12. R.Precharyutasin, V.Pavarajarn and P.Praserthdam, “Effects of the Reaction Parameters on the Carbothermal Reduction and Nitridation of Rice Husk Ash for Silicon Nitride Synthesis”.

3.1.3 International Symposium on Nanotechnology in Environmental Protection and Pollution (ISNEPP 2005), Bangkok, January 12 – 14, 2005

1. J. Klongdee, W. Petchkroh, K. Phuempoonsathaporn, P. Prasertdam, A.S. Vangnai, and V. Pavarajarn, “Activity of Nanosized Titania Synthesized from Thermal Decomposition of Titanium (IV) n-Butoxide for the Photocatalytic Degradation of Diuron”

3.1.4 Regional Symposium on Chemical Engineering (RSCE 2005) Hanoi Horison Hotel, Hanoi, VIETNAM (November 30th –December 2nd, 2005)

1. Rungroj Chanchairoek , Piyasan Praserthdam , Pitt Supaphol ,and Varong Pavarajarna) “Effect of Synthesis and Calcination Parameters on Cristobalite Nanofibers by Combined Sol-Gel and Electrospinning Techniques”
2. Garun Tanarungsuna, Suttichai Assabumrungrata, ,Worapon Kiatkittipongb,

Piyasan Praserthdama, Hiroshi Yamadac *and* Tomohiko Tagawac “Direct hydroxylation of benzene to phenol with hydrogen peroxide catalyzed by Fe/TiO2”

3. Teerawut Ruangsanama, Okorn Mekasuwandumrongb, Piyasan Praserthdama and Varong Pavarajarna, “Physical and Optical Properties of Gallium-Doped Zinc Oxide Nanoparticles Synthesized via Glycothermal Method”
4. Kanyaluck Kontapakdee, Joongjai Panpranot, and Piyasan Praserthdam “Effect of Titania Polymorph on the Characteristics and Catalytic Properties of Pd/TiO2 in Selective Hydrogenation of Acetylene”
5. Kunnika Phandinthong, Joongjai Panpranot, Wandee Luesaiwong, and Piyasan Praserthdam, “A Comparative Study of Liquid Phase Hydrogenation on Pd/SiO2 in Organic Solvents and Under Pressurized Carbon Dioxide”

3.1.5 Technology and Innovation for Sustainable Development Conference (TISD 2006), 25-27 January 2006 Khon Kaen, Thailand

1. Songphol Angkapipattanachai, Thanapon Sangvanich, Pawin Boonyaporn, Joongjai Panpranot*, and Piyasan Praserthdam “Study of Acetylene Hydrogenation Catalysts: Role of Coke Deposits”

3.1.6 Regional Symposium on Chemical Engineering (RSCE 2006) Singapore, (December 3-5, 2006)

1. Terachai Sirikajorn* and Joongjai Panpranot “Synthesis and Catalytic Behavior of Pd supported on nanocrystalline $ZnAl_2O_4$ in Liquid-Phase Semihydrogenation”
2. Patcharaporn Weerachawanasak* and Joongjai Panpranot+ Characteristics and catalytic properties of micron- and nano-sized TiO_2 supported Pd catalysts in liquid-phase hydrogenation of phenylacetylene
3. Sirima Somboonthanakij[a,*], Joongjai Panpranot+, and Okorn Mekasuwandumrong[b] “Characteristics and Catalytic Properties of Nano-Pd/SiO_2 Catalysts Prepared by Flame Spray Pyrolysis”
4. Pimchanok Tupabut, Bunjerd Jongsomjit, and Piyasan Prasethdam, “Characterization of Co/SiO_2-B catalyst and catalytic properties during CO hydrogenation”.
5. Nithinart Chitpong, Bunjerd Jongsomjit, and Piyasan Praserthdam, “Effect of boron-modified zirconia-supported cobalt catalysts and their catalytic properties via CO hydrogenation”.

6. Thidarat Boosamsaiy, Bunjerd Jongsomjit and Piyasan Praserthdam, “Study of cobalt dispersion on the nanoscale Al_2O_3 and SiO_2 supports”.
7. Sirinlak Bunchongturakarn, Bunjerd Jongsomjit, and Piyasan Praserthdam, “Impact of MCM-41 pore structure on ethylene/1-octene copolymerization using MCM-41-supported dried MMAO with zirconocene catalyst”.
8. Chanathip Desharun, Bunjerd Jongsomjit, and Piyasan Praserthdam, “Synthesis of LLDPE-Al_2O_3 polymer nanocomposites via in situ polymerization with zirconocene catalyst”.
9. Supaluk Jiamwijitkul, Bunjerd Jongsomjit, and Piyasan Praserthdam, “Copolymerization behaviors of ethylene/1-octene via boron-modified MCM41-supported zirconocene catalyst”.
10. Chanintorn Ketloy, Bunjerd Jongsomjit, and Piyasan Praserthdam, “Supporting effect of [*t*-BuNSiMe_2Flu]TiMe_2 complex during ethylene/1-octene copolymerization”.
11. Akawat Sirisuk and Kulapong Boonyawes, “Improving efficiency of dye-sensitized solar cell by modification of TiO_2 electrode layer”.
12. Akawat Sirisuk and Sutthirut Charatsaengchirachot, “Synthesis of TiO_2 hollow spheres using spraying technique”.
13. Akawat Sirisuk and Sorathon Wattanamalachai, “Novel method for deposition of copper on zinc oxide by using supercritical carbon dioxide”.
14. Akawat Sirisuk, Prasert Pavasant, and Narakorn Chanprasert, “Photocatalytic degradation of organic dyes using TiO_2 in an air-lift reactor”.

3.1.7 The 4rd Asia-Pacific Congress on Catalysis (APCAT4), December 6-8, 2006, Singapore

1. Nitikon Wongwaranon, Joongjai Panpranot, and Piyasan Praserthdam “Effect of Ni-modified Al_2O_3 on the Properties of Pd/α-Al_2O_3 Catalysts in Selective Hydrogenation of Acetylene”
2. Akawat Sirisuk, Peerapon Buakaew, and Piyasan Praserthdam, “Photocatalytic oxidation of ethylene over gold-deposited titanium dioxide nanoparticles.

3.2 การเชื่อมโยงทางวิชาการกับอุตสาหกรรม

3.2.1 ความร่วมมือกับบริษัทบางกอกโพลีเอททีลีน จำกัด (มหาชน)

ตั้งแต่เริ่มโครงการวิจัยนี้ศูนย์เชี่ยวชาญฯ ได้มีการติดต่อประสานงานกับนักวิจัยของศูนย์วิจัยและพัฒนาของบริษัทฯ คือ ดร. จริยา แซ่จาว และคุณนุชนันท์ อุทัยรัตน์ ซึ่งเป็นหัวหน้าแผนกประกันคุณภาพ ฝ่ายผลิตและวิศวกรรม บริษัทบางกอกโพลีเอททีลีน โดยแผนงานที่ได้ดำเนินการไปแล้ว คือ การให้ความช่วยเหลือและความร่วมมือในการสังเคราะห์ตัวเร่งปฏิกิริยาเมทัลโลซีน (Metallocene catalysis) ที่เป็นสารประกอบเชิงซ้อนของโลหะไทเทเนียมซึ่งมีความว่องไวต่อปฏิกิริยาพอลิเมอร์ไรเซชันของพอลิโอเลฟิน การเตรียมตัวเร่งปฏิกิริยาชนิดนี้เป็นสิ่งที่ยากเนื่องจากสารมัธยันห์ (Intermediates) ที่เกิดขึ้นจะมีความว่องไวต่อสิ่งเจือปน (Impurity) ความชื้น และอากาศ อย่างไรก็ตามเนื่องจากทางศูนย์เชี่ยวชาญฯ เองก็ได้มีความร่วมมือกับผู้เชี่ยวชาญต่างประเทศอยู่แล้ว คือ Professor Takeshi Shiono ณ Hiroshima University ประเทศญี่ปุ่น ภายใต้โครงการการถ่ายทอดเทคโนโลยีไทย-ญี่ปุ่น (Thailand-Japan Technology Transfer Project) ทำให้ได้รับคำแนะนำและเทคนิคในการเตรียมที่ดี ทั้งนี้จากความร่วมมือดังกล่าวทางบริษัทฯ จำกัดได้ส่งนักวิจัยของบริษัทมาเรียนรู้และทำการสังเคราะห์ตัวเร่งปฏิกิริยาเมทัลโลซีนดังกล่าวที่ห้องปฏิบัติการของศูนย์ฯ ในปัจจุบันการเตรียมตัวเร่งปฏิกิริยาดังกล่าวได้บรรลุผลตามเป้าหมายที่วางไว้แล้ว

ในช่วงที่ระยะเวลาหกเดือนที่ผ่านมาศูนย์ฯ ได้ส่งนิสิตปริญญาโทซึ่งได้รับทุนการศึกษาในระดับมหาบัณฑิตจากบริษัทฯ คือ นายสนธยา ศรีจำนอง ไปทำวิจัยที่บริษัทในช่วงปิดเทอมที่ผ่านมา (ตุลาคม - พฤศจิกายน 2549) โดยนิสิตได้ทำการสังเคราะห์ตัวเร่งปฏิกิริยาเมทัลโลซีน คือ สารประกอบเชิงซ้อน Bis[*N*-(3-*tert*–butylsalicylidene)anilinato] zirconium(IV) dichloride ที่มีหมู่ลิแกนด์เป็นกลุ่มของ Phenoxy-Imine โดยมีตัวโลหะเซอร์โคเนียม (Zr) เป็นโลหะอะตอมกลางสำหรับกระบวนการ Ethylene Polymerization ซึ่งมีการตั้งชื่อเป็นกลุ่ม FI catalyst จากการศึกษาที่ผ่านมาพบว่ากลุ่ม FI catalyst นี้จะให้ค่า activity ของกระบวนการ Ethylene Polymerization ที่สูงและให้ผลิตภัณฑ์โพลีเอททีลีนที่มีลักษณะแปลกใหม่ เช่น มีน้ำหนักโมเลกุลที่ต่ำจนถึงสูงมาก ดังนั้นจึงมีความเป็นไปได้สูงที่จะนำตัวเร่งปฏิกิริยาชนิดนี้ไปใช้ในทางอุตสาหกรรมต่อไป ขั้นตอนในการเตรียมจะต้องทำการเตรียมลิแกนด์ก่อนแล้วจึงใส่อะตอมกลางลงไป จากนั้นจึงนำไปทดสอบในปฏิกิริยาพอลิเมอร์ไรเซชันของเอทิลีนต่อไป โดยสามารถสรุปขั้นตอนได้ตามรูปข้างล่างดังนี้

ขั้นตอนการสังเคราะห์ลิแกนด์

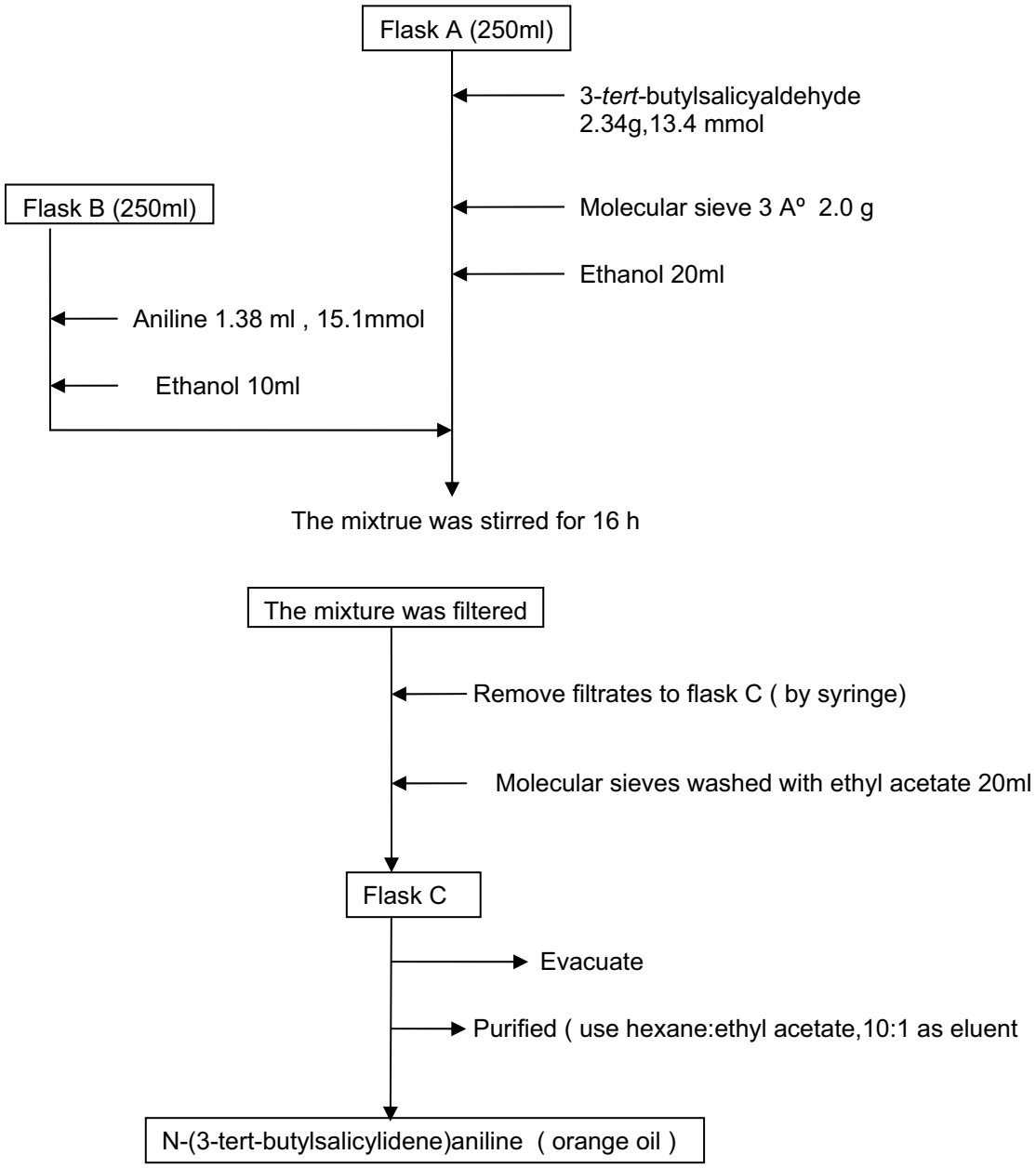

รูปที่ 1 การเตรียมลิแกนด์

ขั้นตอนการเตรียมตัวเร่งปฏิกิริยา

Complex Synthesis (Bis [N-(3-tert-butylsalicylidene) anilinatotitanium(IV)dichloride

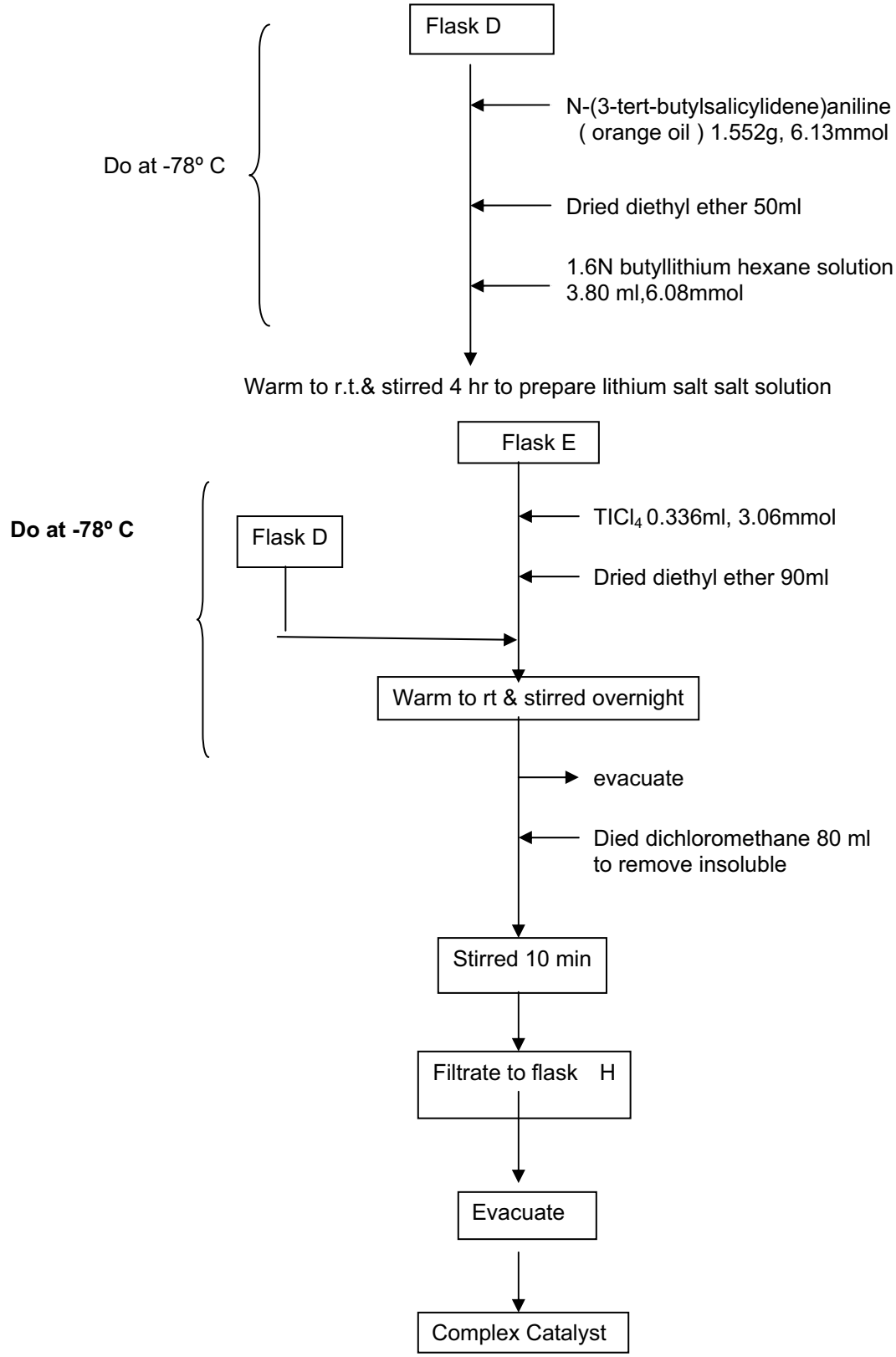

รูปที่ 2 แสดงการเตรียมตัวเร่งปฏิกิริยา

นอกจากการศึกษาสมบัติของตัวเร่งปฏิกิริยาในระบบเอกพันธ์แล้ว ในปัจจุบันยังได้มีการนำตัวเร่งปฏิกิริยาดังกล่าวไปใช้ในระบบวิวิธพันธ์ซึ่งมีตัวรองรับเป็นซิลิกา ไทเทเนีย และออกไซด์ผสมระหว่างซิลิกากับไทเทเนีย เพื่อศึกษาและเก็บข้อมูลต่อไป โดยคาดว่านิสิตจะนำผลวิจัยที่ได้ไปเขียนวิทยานิพนธ์และสำเร็จการศึกษาในระดับมหาบัณฑิตได้ภายในปีการศึกษานี้

3.2.2 ความร่วมมือกับบริษัทระยองโอเลฟินส์ จำกัด
โครงงานปี 2547-2549

โครงการวิจัยร่วมระหว่างศูนย์เชี่ยวชาญเฉพาะทางด้านคาตาไลซิสและวิศวกรรมปฏิกิริยาที่ใช้ตัวเร่งปฏิกิริยาและ บ.ระยองโอเลฟินส์ จำกัด มีวัตถุประสงค์ในการเพิ่มประสิทธิภาพของตัวเร่งปฏิกิริยาสำหรับปฏิกิริยาไฮโดรจิเนชันของอะเซทิลีนซึ่งเป็นขั้นตอนหนึ่งที่สำคัญในกระบวนการผลิตพอลิเอทิลีน โดยปฏิกิริยาไฮโดรจิเนชันของอะเซทิลีนเป็นการกำจัดก๊าซอะเซทิลีนที่ปนเปื้อนในสารตั้งต้น (เอทิลีน) ออกก่อนที่จะเข้าสู่การทำปฏิกิริยาพอลิมอไรเซชันไปเป็นพอลิเอทิลีนก๊าซอะเซทิลีนที่ปนเปื้อนนี้นอกจากจะไปทำให้ความว่องไวของตัวเร่งปฏิกิริยาที่ใช้ในปฏิกิริยาพอลิเมอไรเซชันมีค่าลดลงแล้วยังสามารถเกิดสารประกอบที่เป็นอันตราย เช่น เมทัลอะเซทิลิไดน์ ซึ่งทำให้เกิดการระเบิดได้อีกด้วย ดังนั้นการกำจัดอะเซทิลีนให้ลดลงเหลือปริมาณไม่เกิน 5 ppm จึงมีความจำเป็นอย่างยิ่ง ตัวเร่งปฏิกิริยาที่ใช้ในปฏิกิริยาไฮโดรจิเนชันของอะเซทิลีนที่ใช้อยู่ในปัจจุบันของ บ. ระยองโอเลฟินส์ ได้แก่ตัวเร่งปฏิกิริยาแพลเลเดียมบนอะลูมินาที่เสริมด้วยโลหะซิลเวอร์ ($Pd\text{-}Ag/Al_2O_3$)

งานวิจัยสามารถแบ่งเป็นหัวข้อต่างๆได้ดังนี้

1) การเพิ่มประสิทธิภาพของตัวเร่งปฏิกิริยาใหม่ (Fresh $Pd\text{-}Ag/Al_2O_3$ catalyst) โดยการใช้แก๊สไนตรัสในการทรีตท์เมนต์ตัวเร่งปฏิกิริยา $Pd\text{-}Ag/Al_2O_3$ ซึ่งจากการศึกษางานวิจัยที่เกี่ยวข้องพบว่าพบว่าแก๊สดังกล่าวจะไปขัดขวางการดูดซับของเอทิลีนบนพื้นผิวของตัวเร่งปฏิกิริยาทำให้ได้ผลิตภัณฑ์ที่มีค่าการเลือกเกิดของเอทิลีนสูงขึ้นและลดการเกิดอีเทนได้ โดยทำการหาสภาวะที่เหมาะสมในการทรีตท์เมนต์ พบว่าที่การใช้ปริมาณแก๊สไนตรัสระหว่าง 50-100 ไมโครลิตร ที่อุณหภูมิ 90-100°C ทำให้ได้ปริมาณอะเซทิลีนคอนเวอชันและผลิตภัณฑ์เอทิลีนสูงที่สุด

2) การศึกษาผลของโค้กต่อประสิทธิภาพของตัวเร่งปฏิกิริยาและศึกษาแนวทางในการปรับปรุงกระบวนการฟื้นฟูสภาพของตัวเร่งปฏิกิริยาภายหลังจากการใช้งานในปฏิกิริยาอะเซทิลีนไฮโดรจิเนชันพบว่าตัวเร่งปฏิกิริยาที่ผ่านการใช้งานและฟื้นฟูสภาพแล้วโดยทำการเก็บจากจุดต่างๆของเครื่องปฏิกรณ์ C2-Reactor ของโรงงาน ROC มีปริมาณโค้กหลงเหลืออยู่ทำให้ตัวเร่งปฏิกิริยามีประสิทธิภาพลดลง ในการหาสภาวะที่เหมาะสมในการฟื้นฟูสภาพของตัวเร่งปฏิกิริยาได้ศึกษาตัวแปรต่างๆคือ อุณหภูมิ ความเข้มข้นของออกซิเจนและค่า GHSV พบว่าที่อุณหภูมิ 500°C ขึ้นไปจึงจะทำให้เกิดการเผาไหม้โค้กที่สมบูรณ์ ปริมาณความเข้มข้นของออกซิเจนที่เหมาะสม 10-21% ค่า GHSV = 8000-17000 h^{-1} การใช้ออกซิเจนที่ความเข้มข้นต่ำเกินไปและค่า GHSV สูงเกินไปจะทำให้โค้กเผาไหม้ไม่หมดหรือต้องใช้เวลาในการเผาไหม้นานมาก

รูปแสดงตัวอย่างตัวเร่งปฏิกิริยาที่นำมาทดสอบการกำจัดโค้กที่สภาวะต่าง ๆ

3) การศึกษาความเป็นไปได้ในการนำตัวเร่งปฏิกิริยาที่ผ่านการใช้งานและฟื้นฟูสภาพแล้วมาทำการทรีตเมนต์ด้วยแก๊สไนตรัส พบว่าไม่สามารถทำได้ถึงแม้ว่าตัวเร่งปฏิกิริยาจะไม่มีโค้กหลงเหลืออยู่แล้วก็ตาม ได้ทำการทดสอบด้วยเครื่องมือวิเคราะห์ต่าง ๆอาทิ X-ray Diffraction และ X-ray photoelectron spectroscopy พบว่าเมื่อตัวเร่งปฏิกิริยาผ่านกระบวนการฟื้นฟูสภาพที่อุณหภูมิมากกว่า 500°C จะทำให้โลหะซิลเวอร์เกิดการเคลื่อนที่และมีขนาดเล็กลงทำให้สภาพพื้นผิวของตัวเร่งปฏิกิริยาเปลี่ยนไปและไม่สามารถทำการทรีตด้วยแก๊สไนตรัสได้อีก อย่างไรก็ตามถ้าทำการฟื้นฟูสภาพตัวเร่งปฏิกิริยา (ที่ไม่ได้ผ่านการใช้งาน) ที่อุณหภูมิ 300°C จะสามารถเพิ่มประสิทธิภาพโดยการทรีตเมนต์ด้วยแก๊สไนตรัสได้

ผลงานวิจัยบางส่วนได้มีการนำไปเสนอในที่ประชุมวิชาการระดับนานาชาติ Technology and Innovation for Sustainable Development Conference (TISD) 2006 จัดโดยมหาวิทยาลัยขอนแก่นร่วมกับวิศวกรรมสถานแห่งประเทศไทยในพระบรมราชูปถัมภ์ สถานจัดการและอนุรักษ์พลังงานมหาวิทยาลัยขอนแก่น ศูนย์วิจัยและพัฒนาโครงสร้างมูลฐานอย่างยั่งยืน ศูนย์วิจัยด้านการจัดการสิ่งแวดล้อมและสารอันตราย ระหว่างวันที่ 25-27 มกราคม 2549 ในหัวข้อ “Study of Acetylene Hydrogenation Catalysts: Role of Coke Deposits” โดย Songphol Aungkapipattanachai, Thanapon Sangvanich, Pawin Boonyaporn, Piyasan Praserthdam, and Joongjai Panpranot ณ โรงแรมโซฟิเทล จ.ขอนแก่น

โครงงานปี 2549-2550

การกำจัดสารปนเปื้อนอะโรเมติกส์ออกจากสารนอนอะโรเมติกส์ด้วยกระบวนการไฮโดรจิเนชันโดยใช้ตัวเร่งปฏิกิริยา

(Removal of Aromatics Contaminants from Non-Aromatics Stream by Catalytic Hydrogenation Reaction)

- **ความเป็นมาและความสำคัญของเรื่อง**

ตัวทำละลายอินทรีย์จำพวกนอนอะโรเมติกส์มีความสำคัญในอุตสาหกรรมต่าง ๆและมีการใช้งานในปริมาณสูง โครงการนี้ได้พัฒนาขึ้นเนื่องจากบริษัทระยองโอเลฟินส์ จำกัด มีความสนใจที่จะวิจัยและพัฒนาตัวทำละลายขึ้นใช้เองโดยพัฒนาจากผลิตภัณฑ์รองของบริษัท อย่างไรก็ตามในกระบวนการผลิตตัวทำละลายอินทรีย์มักมีสารปนเปื้อนที่เป็นสารอะโรเมติกส์ปนอยู่ปริมาณเล็กน้อยซึ่งสารอะโรเมติกส์นี้มีความเป็นพิษสูง ซึ่งมีความจำเป็นต้องกำจัดออกเพื่อความปลอดภัยในการใช้งานทั้งต่อคนและสิ่งแวดล้อม

โดยทั่วไปการกำจัดสารอะโรเมติกส์ออกจากสารนอนอะโรเมติกส์ทำได้โดยกระบวนการกลั่นแยกแต่วิธีดังกล่าวจำเป็นต้องใช้พลังงานสูงมาก จึงมีความพยายามที่จะหาเทคนิคหรือวิธีอื่นที่มีประสิทธิภาพมากขึ้นและใช้พลังงานน้อยลง จากการศึกษาในเบื้องต้นพบว่ากระบวนการไฮโดรจิเนชันโดยใช้ตัวเร่งปฏิกิริยาเป็นอีกวิธีหนึ่งที่น่าสนใจเนื่องจากมีประสิทธิภาพสูงและไม่จำเป็นต้องใช้พลังงานมาก อย่างไรก็ดี เพื่อเป็นการพัฒนาเทคโนโลยีขึ้นเองภายในประเทศ ลดภาระการพึ่งพาและค่าใช้จ่ายการในการซื้อเทคโนโลยีจากต่างประเทศ ทางบริษัท ระยองโอเลฟินส์ จึงสนใจที่จะทำวิจัยร่วมกับภาควิชาวิศวกรรมเคมี จุฬาลงกรณ์มหาวิทยาลัยในการพัฒนากระบวนการกำจัดสารปนเปื้อนอะโรเมติกส์ออกจากสารนอนอะโรเมติกส์ด้วยกระบวนการไฮโดรจิเนชัน โดยมุ่งเน้นให้ศึกษาปัจจัยต่าง ๆเช่น ชนิดและปริมาณของตัวเร่งปฏิกิริยา อุณหภูมิ และความดันในการเกิดปฏิกิริยา ซึ่งผลที่ได้จากการศึกษาครั้งนี้จะใช้เป็นแนวทางในการออกแบบเตาปฏิกรณ์และระบบควบคุมปฏิกิริยาไฮโดรจิเนชันสำหรับการกำจัดสารอะโรเมติกส์ออกจากสารนอนอะโรเมติกส์ต่อไปเพื่อให้ได้ประสิทธิภาพในการผลิตตัวทำละลายสำหรับใช้ในกระบวนการต่าง ๆที่เป็นมิตรต่อสิ่งแวดล้อมและใช้พลังงานน้อย

- **วัตถุประสงค์ของโครงงาน**

ศึกษาผลของตัวเร่งปฏิกิริยา อุณหภูมิ และความดันที่มีต่อการเกิดปฏิกิริยาไฮโดรจิเนชันเพื่อการกำจัดสารปนเปื้อนอะโรเมติกส์ออกจากสารนอนอะโรเมติกส์ในกระบวนการผลิตตัวทำละลาย

- **ผลที่คาดว่าจะได้รับ**

ก. สามารถพัฒนากระบวนการกำจัดสารปนเปื้อนอะโรเมติกส์ออกจากสารนอนอะโรเมติกส์แทนการกลั่นแยกเพื่อลดการใช้พลังงานและสามารถหาสภาวะการทำงานที่เหมาะสมเพื่อใช้ในการออกแบบเตาปฏิกรณ์และหน่วยแยกที่คุ้มค่าต่อการลงทุนมากที่สุด

ข. สามารถนำผลิตภัณฑ์รองของบริษัทไปพัฒนาเป็นผลิตภัณฑ์ที่มีมูลค่าเพิ่มสูงขึ้นและไม่เป็นพิษต่อสิ่งแวดล้อม

ค. เป็นกระบวนการต้นแบบสำหรับการศึกษาการกำจัดสารอะโรเมติกส์ออกจากตัวทำละลาย

ในอุตสาหกรรมอื่นๆ

- **แผนการทำงาน**

- ออกแบบอุปกรณ์การทดลองให้สามารถรองรับสภาวะการเกิดปฏิกิริยาที่ต้องการศึกษาได้ โดยอุปกรณ์จะต้องประกอบด้วย

ก.เตาปฏิกรณ์ขนาดทดลองและส่วนประกอบต่างๆที่เพียงพอสำหรับการบรรจุตัวเร่งปฏิกิริยาและควบคุมการการป้อนเข้าสารเพื่อทำปฏิกิริยาและสามารถเก็บตัวอย่างสารหลังทำปฏิกิริยามาวิเคราะห์ได้

ข.อุปกรณ์ให้ความร้อนที่สามารถควบคุมและเปลี่ยนระดับของอุณหภูมิในเตาปฏิกรณ์ตามต้องการได้

ค. อุปกรณ์ควบคุมและเปลี่ยนระดับของความดันในเตาปฏิกรณ์ตามต้องการได้

ง. อุปกรณ์วัดอุณหภูมิและความดันในเตาปฏิกรณ์

จ. อุปกรณ์วัดอัตราการไหล

ฉ. พารามิเตอร์ที่ใช้ในการควบคุมคุณภาพหรือประเมินประสิทธิภาพของการเกิดปฏิกิริยา

- ออกแบบการทดลองโดยการประยุกต์หลักการ DOE (Design of Experiment) มาใช้ ซึ่งจะเป็นการออกแบบการทดลองเพื่อการเก็บข้อมูลแบบสุ่มเพื่อตัดผลของตัวแปรที่ไม่ได้ควบคุมออกไปจากการทดลอง

- ทำการทดลองตามที่ออกแบบไว้เพื่อให้ได้ข้อมูลที่เพียงพอในการวิเคราะห์

ก. อิทธิพลของตัวเร่งปฏิกิริยา

ข. อิทธิพลของอุณหภูมิ

ค. อิทธิพลของความดัน

ง. อิทธิพลร่วมของตัวเร่งปฏิกิริยากับอุณหภูมิ

จ. อิทธิพลร่วมของตัวเร่งปฏิกิริยากับความดัน

ฉ. อิทธิพลร่วมของอุณหภูมิกับความดัน

ช. อิทธิพลร่วมของตัวเร่งปฏิกิริยา อุณหภูมิ และความดัน

- วิเคราะห์ผลการวิจัยและอภิปรายร่วมกับโรงงานเพื่อนำไปทดลองปฏิบัติจริง
- ติดตามผลการปฏิบัติ และประเมินผลสำเร็จ
- จัดทำรายงานสรุป

- **งานที่ได้ดำเนินการไปแล้ว**

- สร้างระบบทดสอบปฏิกิริยาไฮโดรจิเนชันในวัฏภาคของเหลวที่ความดันสูง
- ออกแบบการทดลองโดยใช้โปรแกรม MiniTab ตามหลักการของ DOE
- ทดสอบตัวเร่งปฏิกิริยาที่ใช้ทางการค้าจำนวน 3 ชนิด
- ทดสอบปฏิกิริยาที่สภาวะต่างๆตามที่ได้ออกแบบการทดลองไว้

- **ตัวอย่างผลการวิจัย**

อุปกรณ์สำหรับการทดสอบปฏิกิริยาไฮโดรจิเนชันในวัฏภาคของเหลวที่ความดันสูง

ตัวอย่างผลิตภัณฑ์

ผลการทดลองที่สภาวะต่าง ๆโดยใช้หลักการออกแบบการทดลองแบบ 2^5 factorial design

(benzene concentration; A, amount of catalyst; B, hydrogen pressure; C, reaction temperature; D, reaction time; E, and coded value; X.)

Run number	A (°C)	B (bar)	C (minutes)	D (%wt)	E (g)	Benzene Conversion (%)
1	1	5	30	100	30	5.4
2	10	15	30	150	120	20.7
3	10	15	30	100	30	42.0
4	1	15	10	100	30	28.2
5	10	5	30	150	30	5.3
6	1	15	30	150	30	41.6
7	1	5	10	150	30	25.0
8	6	10	20	125	75	23.0
9	6	10	20	125	75	27.6
10	1	15	30	100	120	38.8
11	1	5	30	150	120	100.0
12	1	15	10	150	120	17.2
13	1	5	10	100	120	26.7
14	10	5	10	100	30	5.6
15	10	15	10	100	120	32.3
16	6	10	20	125	75	21.1
17	10	5	10	150	120	20.8
18	10	5	30	100	120	14.8
19	10	15	10	150	30	37.8

ข้อมูลทางสถิติ

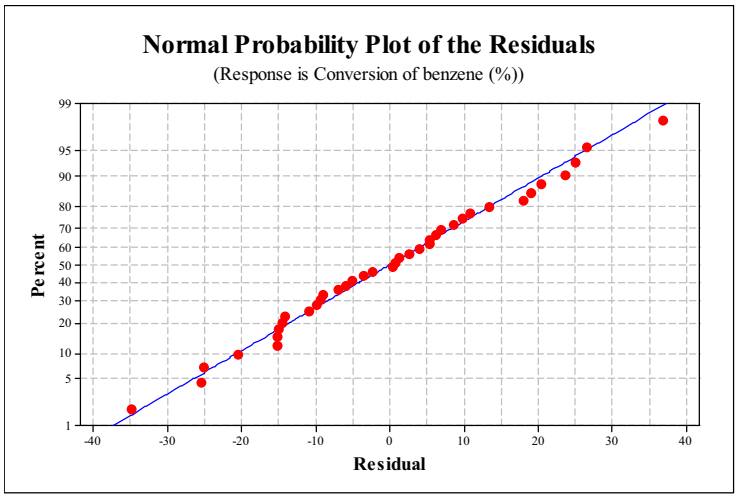
Normal Probability Plot of the Residuals
(Response is Conversion of benzene (%))
Percent
Residual

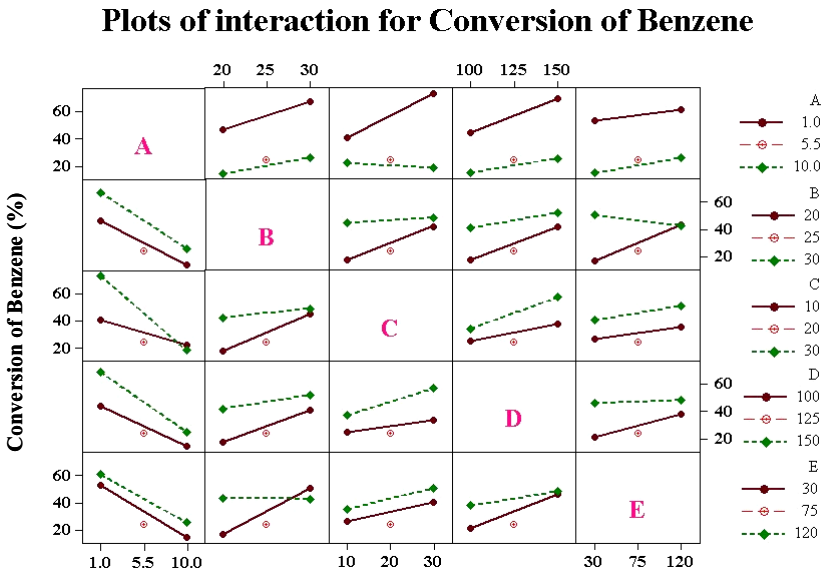
Plots of interaction for Conversion of Benzene
Conversion of Benzene (%)
A
B
C
D
E

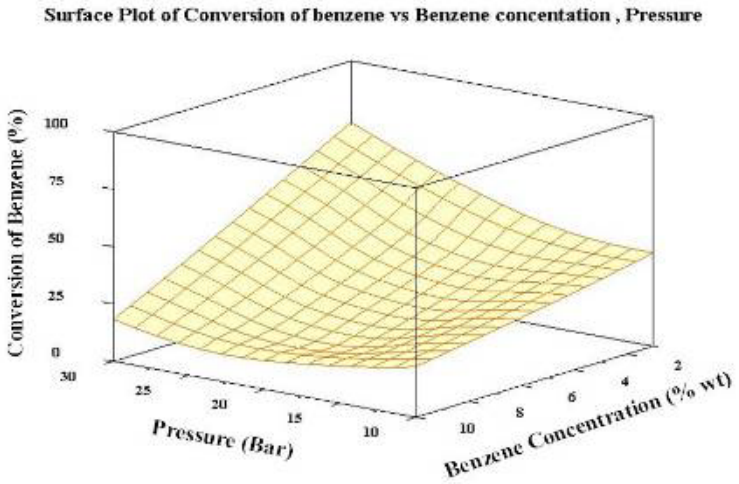
Surface Plot of Conversion of benzene vs Benzene concentation , Pressure
Conversion of Benzene (%)
Pressure (Bar)
Benzene Concentration (% wt)

- **ผลที่ได้รับจากการวิจัย**

ก. สามารถพัฒนากระบวนการกำจัดสารปนเปื้อนอะโรเมติกส์ออกจากสารนอนอะโรเมติกส์แทนการกลั่นแยกเพื่อลดการใช้พลังงานและสามารถหาสภาวะการทำงานที่เหมาะสมเพื่อใช้ในการออกแบบเตาปฏิกรณ์และหน่วยแยกที่คุ้มค่าต่อการลงทุนมากที่สุด

ข. สามารถนำผลิตภัณฑ์รองของบริษัทไปพัฒนาเป็นผลิตภัณฑ์ที่มีมูลค่าเพิ่มสูงขึ้นและไม่เป็นพิษต่อสิ่งแวดล้อม

ค. เป็นกระบวนการต้นแบบสำหรับการศึกษาการกำจัดสารอะโรเมติกส์ออกจากตัวทำละลายในอุตสาหกรรมอื่นๆ

4. การสร้างห้องปฏิบัติการวิจัยในบริษัทเอกชน

ได้ทำสัญญาความร่วมมือในการทำวิจัยกับบริษัท SCG Chemical CO. LTD. โดยมีการสร้างห้องปฏิบัติการวิจัยของบริษัทฯ ในพื้นที่ภายในมหาวิทยาลัย โดยโครงการความร่วมมือคิดเป็นงบประมาณทั้งสิ้น 39 ล้านบาท โดยเริ่มโครงการตั้งแต่วันที่ 9 เมษายน 2550

5. การจัดสัมมนาเพื่อเผยแพร่ผลงานวิจัย

ได้มีการจัดสัมมนาทางวิชาการเพื่อเผยแพร่ผลงานจากทุนส่งเสริมกลุ่มวิจัยในหัวข้อ “การประยุกต์ใช้ตัวเร่งปฏิกิริยาและเครื่องปฏิกรณ์เคมีสำหรับอุตสาหกรรมปิโตรเคมี” ในวันที่ 27 กรกฎาคม 2550 ณ ห้องประชุม ชั้น 2 ตึกเจริญวิศวกรรม อาคาร 4 คณะวิศวกรรมศาสตร์ จุฬาลงกรณ์มหาวิทยาลัย โดยมีผู้เข้าร่วมสัมมนาทั้งสิ้น 68 คน โดยมีรายละเอียดการสัมมนาดังแสดงในเอกสารแนบชุดที่ 39

6. สรุปผลงาน

ตารางที่ 1 สรุปผลงานตามข้อเสนอโครงการและผลงานในรอบ 3 ปี

รายการ	ผลงานตามข้อเสนอโครงการ	ผลงานรวมที่ทำได้
1. การสร้างห้องปฏิบัติการวิจัยในบริษัทเอกชน	1	1
2. การเลือกตัวเร่งปฏิกิริยาที่เหมาะสมสำหรับการใช้งานในทางการค้า	1	2[1]
3. ผลงานตีพิมพ์ในวารสารระดับนานาชาติ	24	42 + 2[2]

4. ผู้สำเร็จระดับปริญญาเอก	9	5 + 8[3]
5. ผู้สำเร็จระดับปริญญาโท	30	48
6. การจัดสัมมนาเผยแพร่ผลงานวิจัย	1	1

หมายเหตุ [1] วิเคราะห์ตัวอย่างให้บริษัท TUNTEX PETROCHEMICALS (THAILAND) PUBLIC COMPANY LIMITED 3 ตัวอย่าง และวิเคราะห์ตัวอย่างให้บริษัทระยองโอเลฟินส์ 8 ตัวอย่าง

[2] จำนวนบทความที่อยู่ระหว่างการแก้ไข

[3] จำนวนนิสิตปริญญาเอกที่จะสำเร็จการศึกษา

ลงนาม

(ศ.ดร. ปิยะสาร ประเสริฐธรรม)
หัวหน้าโครงการ

An Alternative Correlation Equation between Particle Size and Structure Stability of H−Y Zeolite under Hydrothermal Treatment Conditions

Somyod Sombatchaisak,[†] Piyasan Praserthdam,*[,†] Choowong Chaisuk,[‡] and Joongjai Panpranot[†]

Center of Excellence on Catalysis and Catalytic Reaction Engineering, Department of Chemical Engineering, Chulalongkorn University, Bangkok 10330, Thailand, and Department of Chemical Engineering, Faculty of Engineering and Industrial Technology, Silpakorn University, Nakon Pathom 73000, Thailand

The effect of particle size in the range of 0.16−2.01 μm on the hydrothermal stability of H−Y zeolite under hydrothermal treatment conditions similar to those used in FCC processes was investigated. The average particle size of 0.45 μm was found to be the optimum particle size of H−Y zeolite to retain a high percent crystallinity upon hydrothermal treatment. A new correlation was developed by plotting the relative crystallinity (C/C_0) against the reciprocal of the square root of the particle size (d_0) of Y zeolite. The correlation accurately predicts the hydrothermal stability of Y zeolite in small to medium particle sizes for a given temperature. For the larger particle sizes of Y zeolite (>0.45 μm), no exact correlation between particle size and hydrothermal stability was found, probably because of the presence of more structural defects in the zeolite, as shown by higher Brønsted/Lewis acid ratios.

1. Introduction

Fluid catalytic cracking (FCC) produces approximately one-third of the world's gasoline supply using faujasite-type zeolites. The commercial FCC catalysts consist of 1−2-μm Y zeolite embedded in a matrix of 40−80-μm spherical amorphous aluminosilicate particles. While circulating in an FCC unit, zeolites encounter severe hydrothermal conditions, resulting in physical and chemical changes that affect the surface area, pore volume, and catalytic cracking performance of the zeolites. Several factors influencing the hydrothermal stability of Y zeolite have been reported, including the Si/Al ratio,[1] the dealumination procedure,[2−6] and the hydrothermal aging conditions.[7,8] Zeolites with higher hydrothermal stability can be obtained by using higher Si/Al ratios or by incorporating rare earth or noble metals into the zeolite framework to help prevent dealumination upon hydrothermal treatment.[9−12]

Particle size has been found to affect the performance of zeolites for many catalytic reactions. For examples, Rajagopalan et al.[13] studied the effect of the particle size of NaY zeolite in the range of 0.06−0.65 μm on its activity and selectivity in FCC reaction. It was found that catalysts containing smaller-particle zeolites exhibited higher activities in the cracking of gasoil and higher selectivities to gasoline and light cycle oil than those containing larger-particle zeolites. Gianetto et al.[14] found similar results for ultrastable submicron Y (USSY) zeolites. Changes in the zeolite particle size significantly affect the amounts of total aromatics, benzene, C_4 olefins, and coke during FCC. Al Khattaf and de Lasa[15] reported that the cracking conversion of 1,3,5-triisopropylbenzene using 0.4-μm Y zeolite was higher than that obtained using 0.9-μm zeolite because of the constrained diffusional transport in the larger Y zeolite particles. However, smaller-particle zeolites have often been found to be less stable than larger-particle ones. The optimum size of the zeolite crystal is, therefore, required to achieve the desired performance.[16,17] In a previous study reported by our laboratory, Praserthdam et al.[18] investigated the effect of crystal size on the durability of Co/HZSM-5 in the selective reduction of NO. The Co/HZSM-5 with the smaller crystal size showed the greater durability. The critical diameter of the crystal size of Co/HZSM-5 for this reaction was determined to be 2 μm.

In this study, an alternative correlation between the particle size and structure stability of H−Y zeolite under hydrothermal treatment conditions is developed. The effects of particle size and hydrothermal conditions similar to those used in the FCC process on the structural changes of Y zeolite were investigated by means of X-ray diffraction (XRD), BET surface area measurements, nuclear magnetic resonance (NMR) spectroscopy, scanning electron microscopy (SEM), temperature-programmed desorption (TPD) of NH_3, and Fourier transform infrared (FTIR) spectroscopy of adsorbed pyridine.

2. Experimental Section

2.1. Preparation of H−Y Zeolite Catalysts. H−Y zeolite catalysts with different particle sizes in the range of 0.16−2.01 μm were prepared in our laboratory according to the method of Miyanohara et al.[19] The Si/Al ratio of 4.5 was used for all catalyst samples. The initial materials for the synthesis of zeolite Y are sodium silicate (Merck), sodium hydroxide (Merck), sodium aluminate (Fuka), and distilled water. The molar composition of the gel was 3.68 Na_2O/1 Al_2O_3/12 SiO_2/148 H_2O. The gel was aged at room temperature for various aging times (0.5, 2, 4.5, or 6.5 days). Then, it was heated to a specified temperature (363, 373, or 383 K) in an

* To whom correspondence should be addressed. Tel.: +662-218-6766; Fax: +662-218-6769 E-mail: piyasan.p@chula.ac.th.
[†] Chulalongkorn University.
[‡] Silpakorn University.

10.1021/ie049847k CCC: $27.50
Published on Web 06/11/2004

oven for 24 h. After being cooled to ambient temperature, the sample was washed thoroughly several times with deionized water until the pH was 7. The obtained samples were dried at 383 K overnight and calcined at 773 K in an air flow for 2 h. The hydrogen form of Y zeolite was then obtained by first exchanging Na^+ with NH_4^+ using an aqueous solution of NH_4NO_3 and subsequently decomposing the NH_4^+ by calcination in air at 773 K for 2 h.

2.2. Hydrothermal Treatment. Hydrothermal treatment of the catalysts was performed in a homemade system. Approximately 0.5 g of catalyst sample was placed in the reactor and was first heated in a nitrogen flow to the specified temperature (873, 973, 1073, 1173, or 1273 K) using a ramp rate of 10 K/min. The sample was kept at this temperature for a specified time period (0.5, 1, 2, 3, or 5 h) while steam at different partial pressures (0.05, 0.1, 0.2, 0.5, or 1.0) was added. Finally, the sample was cooled to room temperature in a nitrogen stream.

2.3. Catalyst Characterization. 2.3.1. Scanning Electron Microscopy (SEM). The average particle sizes and particle size distributions of the catalysts before and after hydrothermal treatment were determined visually from SEM micrographs obtained using a JEOL JSM-35 CF model scanning electron microscope.

2.3.2. BET Surface Area Analysis. The specific surface areas of the samples were calculated using the Brunauer–Emmett–Teller (BET) single-point method. Approximately 0.3–0.5 g of the catalyst sample was placed in the sample cell, heated to 473 K, and held at that temperature for 10 h under a 30% N_2/He flow. The catalyst sample was then cooled to room temperature and dipped into liquid nitrogen. After the adsorption of nitrogen reached equilibrium, the sample cell was then dipped into a water bath at room temperature. The amount of nitrogen desorbed was measured by a gas chromatograph (GOW-MAC).

2.3.3. X-ray Diffraction (XRD). X-ray diffraction patterns of the catalysts were obtained using a Seimens D5000 X-ray diffractometer with monochromatized Cu Kα radiation (10 kV, 20 mA). The relative crystallinity was estimated by comparing the peak intensities of the treated samples with those of fresh samples. The total intensities of the eight peaks assigned to the (331), (511), (440), (533), (642), (822), (555), and (664) reflections were used for comparison according to ASTM D3906 method.

2.3.4. Nuclear Magnetic Resonance (NMR) Spectroscopy. The chemical state of Al was measured by ^{27}Al MAS NMR spectroscopy using a Bruker DPX-300 NMR spectrometer operated at 78.2 MHz at the magic angle. The relative area of tetrahedral ^{27}Al was calculated from the area of tetrahedral aluminum per summation area of tetrahedral and octahedral aluminum.

2.3.5. NH_3 Temperature Program Desorption (NH_3 TPD). The amount of acidic sites on the catalysts was measured using the NH_3 temperature-programmed desorption (TPD) technique. Approximately 0.25 g of Y zeolite catalyst was placed in a U-shape quartz tube, incorporated in a temperature-controlled oven, and connected to a thermal conductivity detector (TCD). Prior to ammonia adsorption, the catalyst was first heated to 773 K at a ramp rate of 10 K/min in a nitrogen flow and held at this temperature for 1 h to remove any remaining water or other organic compounds. It was then cooled to 353 K before saturation of catalyst surface with ammonia using 10% NH_3/He (high purity grade, Thai Industrial Gas Co., Ltd.) at a flow rate of 60 mL/min.

The temperature-programmed desorption was performed with a constant heating rate of ca. 10 K/min from 363 to 973 K. The amount of NH_3 desorbed was measured by analyzing the effluent gas with a thermal conductivity detector.

2.3.6 Fourier Transform Infrared (FTIR) Spectroscopy. IR spectra of adsorbed pyridine were recorded to distinguish and measure the two types of acidic sites on the zeolite surface, i.e., Lewis and Brønsted acid sites. FTIR experiments are performed on a Nicolet model Impact 400 instrument with deuterated triglycine sulfate (DTGS) detector in the same manner as used by Linjie et al.[20] Approximately 0.06 g of catalyst powder was pressed into wafers (1 cm in diameter) and pretreated in a vacuum of 10^{-4} Torr at room temperature for 1 h. Then, pyridine was introduced into the IR cell by self-vaporizing in a vacuum and was circulated through the system by electromagnetic pump. After saturation, the adsorbed pyridine was evacuated at room temperature for 5 h or until no change in IR spectrum was observed. Then, FTIR measurement of the spectrum of the pyridine-adsorbed sample was started at room temperature.

Table 1. Effect of Preparation Conditions on the Average Particle Size of HY Zeolite

aging time (day)	reaction temperature (K)	average particle size (μm)[a]
0.5	363	1.19
	373	amorphous
	383	amorphous
2.0	363	0.82
	373	1.81
	383	2.01
4.5	363	0.31
	373	0.45
	383	0.40
6.5	363	0.16
	373	0.25
	383	0.45

[a] Average particle size was evaluated using SEM. Measurement error = ±5%.

3. Results and Discussion

3.1. Effect of Preparation Conditions on Particle Size of H–Y Zeolite. The Y zeolites with different particle sizes ranging from 0.16 to 0.21 μm used in this study were prepared by varying the aging time of nucleation and the gel reaction temperature. The average particle sizes of the Y zeolites obtained under various synthesis conditions are reported in Table 1. Reaction temperatures in the range 363–383 K were found to be optimum for producing Y zeolite.[21] The minimum time required to obtain a zeolite crystal structure was determined to be ca. 2 days; otherwise, amorphous materials were produced. It was found that lower reaction temperature (lower crystal growth rate) and longer aging time of nucleation resulted in smaller zeolite crystals. A similar result was reported by Zhdanov et al.[8] for the synthesis of Na–A zeolite. Typically, the particle size of zeolites depends on the relative rates of the two competing phenomena occurring during synthesis, namely, nucleation and crystal growth. Both rates decrease with decreasing temperature;[22] however,

Table 2. Characteristics of HY Zeolite before and after the Hydrothermal Treatment[a]

particle size[b] (μm)		BET surface area[c] (m^2/g)		
before	after	before	after	relative BET SA (%)
0.16	0.16	521	322	38
0.31	0.31	546	366	33
0.45	0.45	511	441	14
0.82	0.82	531	397	25
2.01	2.01	550	339	38

[a] Treatment conditions were 1073 K, 10 mol % steam, and 1 h. [b] Average particle size was evaluated using SEM. Measurement error = ±5%. [c] Measurement error = ±10%.

the impact of decreasing temperature is more pronounced on the crystal growth rate than on the nucleation rate, resulting in smaller particle size at lower temperature.[23] Another factor influencing the size of zeolite crystals is the aging time of nucleation. The longer the aging time of nucleation, the lower the uniformity of nucleus precursors in the reaction mixture, and consequently, the smaller the zeolite particles formed.[24]

3.2. Effect of Hydrothermal Treatment on the Physical Properties of H−Y Zeolite. The particle sizes and BET surface areas of Y zeolites before and after hydrothermal treatment are reported in Table 2. The Y zeolites prepared under different preparation conditions resulted in spherical particles with average particle sizes varying from 0.16 to 2.01 μm. The particle sizes and shape remained unaltered after the samples underwent hydrothermal treatment at 1073 K and 10 mol % steam for 1 h. It is known that the BET surface area of Y zeolite decreases upon hydrothermal treatment because of the collapse of the zeolite framework.[25] However, in this study, it was found that changes in BET surface areas were more pronounced for smaller- or larger-particle-size Y zeolites compared to the medium-particle-size samples (0.45 μm).

The crystallinity of Y zeolite was also affected during hydrothermal treatment as a result of aluminum extraction and dehydroxylation.[26] Figure 1a−c shows the effect of particle size on the crystallinity of Y zeolite when the aging parameters are varied as follows: (a) temperature (873−1273 K), (b) aging time (30−300 min), and (c) steam partial pressure (5−100%). The relationships between the percent crystallinity and the particle size of Y zeolite when the aging parameters are varied follow similar volcano trends. The percentages of crystallinity decreased significantly with increasing hydrothermal temperature, steam partial pressure, and aging time, which is typical hydrothermal behavior for zeolites in FCC catalysts.[2] In this study, the lowest percent crystallinity was observed for the most severe hydrothermal conditions (1273 K, 100% steam partial pressure, and 300 min).

The hydrothermal stability of the Y zeolites was also found to be strongly dependent on their particle size. For the particle sizes ranging from 0.16 to 0.45 μm, the percent crystallinity increased with increasing particle sizes, and the maximum percent crystallinity of ca. 80−90% was observed for the particle size of 0.45 μm. This trend is in agreement with the literature findings that smaller-crystallite zeolites are more active but less stable than those with larger crystallites.[27,28] The percent crystallinity of the Y zeolites, however, gradually decreased for particle sizes larger than 0.45 μm. The hydrothermal behavior of larger-particle Y zeolite

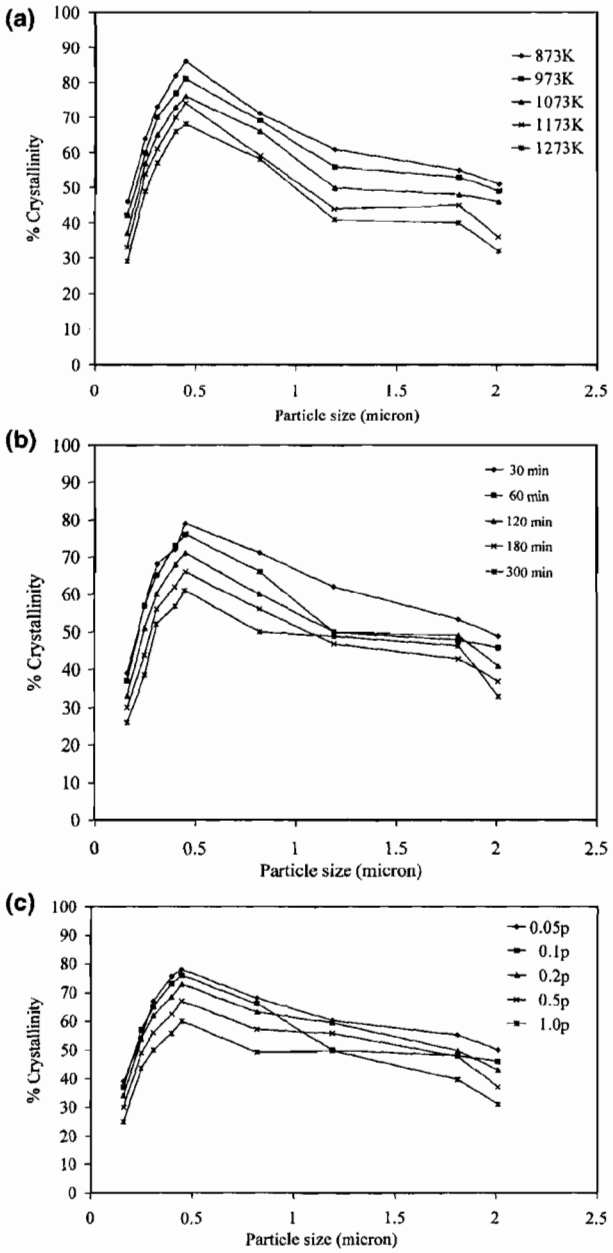

Figure 1. Relationship between percent crystallinity and particle size of Y zeolite after hydrothermal treatment with different treatment parameters: (a) 873−1273 K, 10 mol % steam, and 60 min; (b) 30−300 min, 10 mol % steam, and 1073 K; (c) 0.05−1 P/P_0, 60 min, and 1073 K. Measurement error was ±5%.

is still unclear; however, the decrease in percent crystallinity is probably due to a larger amount of defects in larger-particle-size Y zeolite. In addition, there might be an influence from the average distance between acidic and metallic sites[29] or the various pore sizes in large-particle shape-selective zeolite. In a previous study, Praserthdam et al.[18] reported that the larger-particle Co/HZSM-5 catalysts experienced significant losses of crystallinity and tetrahedral aluminum upon hydrothermal treatment whereas those characteristics for the smaller-particle catalysts remained unaffected.

3.3. Dealumination after Hydrothermal Treatment. ^{27}Al MAS NMR spectra for all of the catalyst samples in this study were collected. Figure 2a−c shows

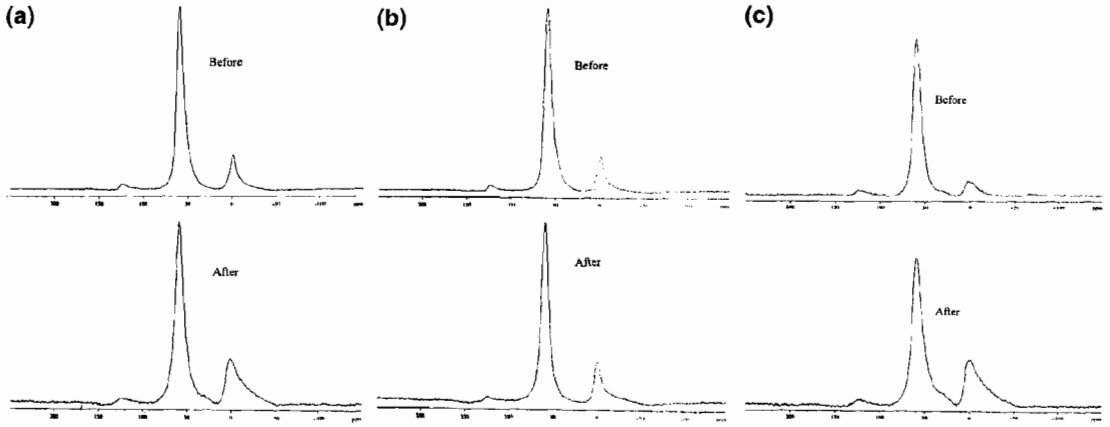

Figure 2. ^{27}Al MAS NMR spectra of Y zeolite fresh samples with the different average particle sizes (a) 0.16, (b) 0.45, and (c) 0.82 μm before and after hydrothermal treatment at 1073 K, 10 mol % steam, and 1 h.

Table 3. Relative Areas of ^{27}Al NMR Peaks and Acid Properties of HY Zeolite with Various Particle Sizes

particle size (μm)	relative area of tetrahedral ^{27}Al[a]		acid site[b]		ratio of B/L[c]
	before	after	Brønsted	Lewis	
0.16	83.69	69.14	62	201	0.31
0.31	85.06	77.99	86	245	0.35
0.45	84.52	83.63	79	243	0.33
0.82	90.64	78.97	120	259	0.46
2.01	94.63	71.35	189	284	0.67

[a] Relative area of tetrahedral ^{27}Al was calculated from the area of tetrahedral aluminum per summation area of tetrahedral and octahedral aluminum. Measurement error = ±10%. [b] Acid site was calculated using the area of the Brønsted band at 1540 cm^{-1} and the area of Lewis band at 1450 cm^{-1} from FTIR experiments. [c] Ratio of B/L was calculated from area of Brønsted sites per area of Lewis sites.

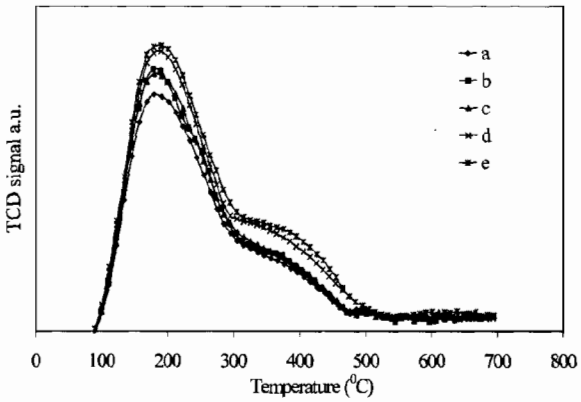

Figure 3. NH_3 TPD of fresh Y zeolite at various particle sizes: (a) 0.16, (b) 0.31, (c) 0.45, (d) 0.82, and (e) 2.01 μm.

the ^{27}Al MAS NMR spectra of Y zeolites with particle sizes of 0.16, 0.45, and 2.01 μm before and after hydrothermal aging. In the fresh samples, a strong signal at ca. 56 ppm and a weak signal at ca. 0 ppm were detected. These peaks correspond to tetrahedrally coordinated Al species (Al^{IV}) in the zeolitic framework and octahedrally coordinated extraframework Al (Al^{VI}), respectively.[30,31] After hydrothermal aging at 1073 K for 1 h, a decrease in tetrahedral aluminum and an increase in octahedral aluminum were observed for Y zeolites in all particle sizes used in this study except for the medium size (0.45 μm). The loss in crystallinity is due to framework dealumination of the zeolite.[18,31] For strongly dealuminated samples, another peak or a small shoulder is often visible between 30 and 50 ppm in the ^{27}Al MAS NMR spectra, which has been assigned to pentacoordinated aluminum atoms[32] or distorted tetrahedrally coordinated aluminum atoms in extraframework species.[33-34]

The relative areas of tetrahedral ^{27}Al before and after hydrothermal treatment are reported in Table 3. They were found to be in accordance with the percentages of crystallinity. Medium-particle-size Y zeolite (0.45 μm) exhibited the lowest amount of dealumination; subsequently, the highest percent crystallinity was obtained with these samples.

3.4. Characterization of Acidic Sites. The NH_3 temperature-programmed desorption (TPD) technique provides information on the amount and strength of acidic sites. The peak area of a TPD profile represents the amount of desorbed NH_3, whereas the peak position corresponds to the strength of acidity. The NH_3 TPD profiles of Y zeolites with various particle sizes are shown in Figure 3. All catalyst samples exhibited similar TPD profiles. The first desorption peak at ca. 473 K is assigned to the weak acid sites, whereas the second peak at ca. 653 K corresponds to strong acid sites.[35] The amount of weak acid sites was determined to be much higher than the amount of strong acid sites. Interestingly, higher amounts of strong acid sites were detected on larger-particle-size of Y zeolite.

Pyridine adsorption IR spectroscopy is another powerful technique for measuring and distinguishing the acidic sites on a zeolite surface. Figure 4 shows the pyridine adsorption behaviors of fresh Y zeolites with different particle sizes. The two bands at ca. 1450 and 1540 cm^{-1} are assigned to pyridine molecules adsorbed on Lewis acid sites and Brønsted acid sites, respectively. The integrated areas of the bands are proportional to the numbers of corresponding acid sites. The type of acid sites has been found to depend on the synthesis conditions. Kumar et al.[36] reported that fresh H−ZSM-5 catalysts synthesized at the longest aging time used in the study exhibited the highest number of Brønsted acid sites. The ratio of Brønsted to Lewis (B/L) acid sites, as well as the relative area of ^{27}Al obtained from ^{27}Al MAS

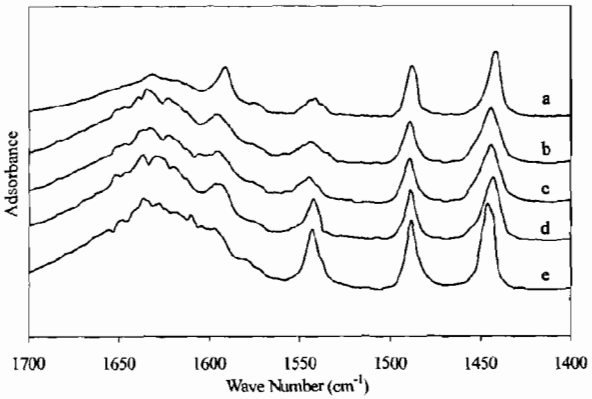

Figure 4. Pyridine adsorption at room temperature of fresh Y zeolite with various particle sizes: (a) 0.16, (b) 0.31, (c) 0.45, (d) 0.82, and (e) 2.01 μm.

NMR spectra, as functions of the particle size of Y zeolites are summarized in Table 3. All Y zeolite catalyst samples contained both Lewis and Brønsted acid sites with higher amounts of Lewis acid sites than Brønsted acid sites. It was found that the larger-particle-size Y zeolites exhibited higher Brønsted/Lewis acid site (B/L) ratios than the smaller-particle-size ones. The results from FTIR spectroscopy are in accordance with the NH_3 TPD results that higher amounts of strong acid sites were detected on larger-particle Y zeolites.

Because a significant loss of crystallinity and a high level of Bronsted acid sites were observed for larger particles, it is suggested that more defects in larger particles might result in the difference in acidity and play a role in crystallinity loss upon hydrothermal treatment. The higher amount of Bronsted acid sites has been ascribed to a higher density of hydroxyl groups.[37] A shorter distance between hydroxyl groups increases the probability of dehydroxylation and dealumination resulting in loss of crystallinity.

3.5. Correlation between Particle Size and Hydrothermal Stability of Y Zeolites. The hydrothermal stability of the Y zeolites was determined in terms of changes in crystallinity (C/C_0) where C_0 is the catalyst's initial crystallinity and C is the crystallinity observed after hydrothermal treatment. Figure 5a–c shows plots of C/C_0 vs $1/(d_0)^{1/2}$, where d_0 is the particle size of the Y zeolite, for different hydrothermal treatment conditions: (a) 0.1 steam partial pressure, 60 min, 873–1273 K; (b) 0.1 steam partial pressure, 1073 K, 30–300 min; and (c) 1073 K, 60 min, 0.1–1.0 steam partial pressure. It was found that all of the plots exhibit the same characteristics consisting of two parts. The first parts represent the correlation between hydrothermal stability and particle size for larger particles and have irregular shapes, whereas the second parts represent the correlation for the smaller particles and show fairly the same linear trend. The irregular shape in the first part of each figure was probably caused by structure defects as stated in a preceding paragraph.

However, the existence of the linear trend in the second part of Figure 5a provides new insight into the effect of particle size on the hydrothermal stability of Y zeolite. The hydrothermal stability of Y zeolite can be predicted from particle size and operating temperature using the following empirical correlation of observed changes in zeolite crystallinity as a function of particle

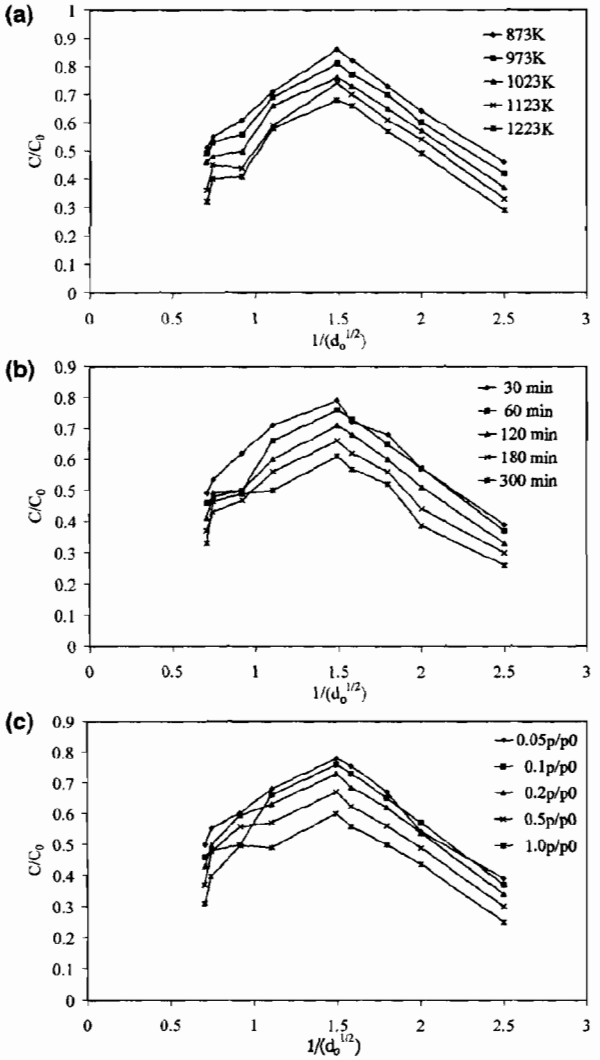

Figure 5. Correlation between C/C_0 and $1/(d_0)^{1/2}$ at different treatment parameters: (a) 873–1273 K, 10 mol % steam, and 60 min; (b) 30–300 min, 10 mol % steam, and 1073 K; (c) 0.05–1 P/P_0, 60 min, and 1073 K.

size and temperature

$$\frac{C}{C_0} = n\left(\frac{1}{\sqrt{d_0}}\right) + f(T) \qquad (1)$$

where C_0 is the catalyst's initial crystallinity, C is the crystallinity observed after hydrothermal treatment, d_0 is the particle size before treatment (μm), n is the slope of the graph, and T is treatment temperature (K). The value of n was determined by averaging the slopes of the graphs. The function of T, $f(T)$, was determined by plotting the intercept values of each plot versus temperature. Therefore, eq 1 can be written as

$$\frac{C}{C_0} = -0.3937\left(\frac{1}{\sqrt{d_0}}\right) + \frac{498}{T} + 0.881 \qquad (2)$$

This correlation was found to correctly predict the hydrothermal stability of Y zeolites of small to medium particle size (0.1–0.45 μm). The square root of the

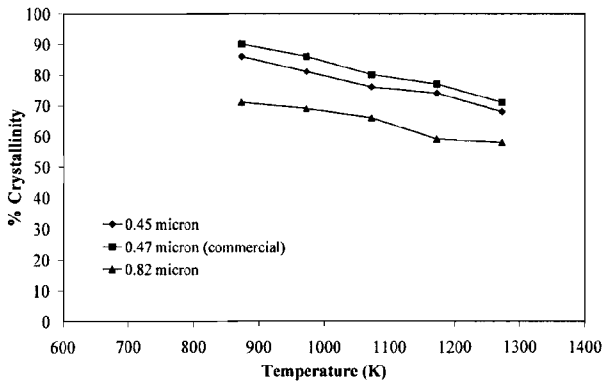

Figure 6. Comparison of the hydrothermal stability of a commercial HY zeolite and the synthesized catalysts (the treatment conditions were 873−1273 K, 10% mol steam, and 1 h).

particle size of the Y zeolite prior to hydrothermal treatment in our correlation probably includes the effects of the nucleus density in amorphous gel at the reaction temperature and/or the initial pseudo-cell concentration in the gel phase as these two factors have been determined to be proportional to the gel reaction temperature and the crystal size during the crystallization of zeolites.[38]

The validity of this correlation was tested by performing the hydrothermal treatment of a commercial Y zeolite catalyst obtained from Tosoh Corporation, Tokyo, Japan, with a particle size of 0.47. The results are shown in Figure 6. Similar profiles were observed for the catalysts prepared in our laboratory and the commercial one. However, for a similar particle size, a slightly higher hydrothermal stability was observed for the commercial catalyst, probably because of a higher Si/Al ratio. Therefore, the correlation proposed in this study might be limited to a Si/Al ratio of 4.5. The results, however, offer interesting possibilities for developing a more versatile correlation that can be applied to Y zeolites with different Si/Al ratios and/or that were prepared under different reaction conditions.

4. Conclusion

The hydrothermal stability of Y zeolite was found to strongly depend on the particle size. The maximum percent crystallinity after hydrothermal treatment was obtained for Y zeolite with a particle size 0.45 μm. By plotting the relative percent crystallinity (C/C_0) versus the particle size of Y zeolite (d_0, μm) in the form of $1/\sqrt{d_0}$ for a given treatment temperature (T, K), an alternative correlation was found

$$\frac{C}{C_0} = -0.3937\left(\frac{1}{\sqrt{d_0}}\right) + \frac{498}{T} + 0.881$$

This correlation can be applied for small to medium particle sizes ranging from 0.1 to 0.45 μm. For larger particle sizes, the defects in the Y zeolite structure, as indicated by higher Bronsted acid site contents, were probably responsible for a decrease in crystal stability upon hydrothermal treatment.

Acknowledgment

The financial support from the Thailand Research Fund (TRF) and TJTTP-JBIC is gratefully acknowledged.

Literature Cited

(1) Dashiti, H.; Albazaz, H. Comparative Study of the Hydrothermal Stability and Performance of Y-Zeolite Based FCC Catalyst Having Differrent Initial Si/Al Ratio. *Fuel Sci. Technol. Int.* **1995**, *13*, 451.

(2) Triantafillidis, C. S.; Vlessidis, A. G.; Evmiridis, N. P. Dealuminated H−Y Zeolites: Influence of the Degree and the Type of Dealumination Method on the Structural and Acidic Characteristics of H−Y Zeolites. *Ind. Eng. Chem. Res.* **2000**, *39*, 307.

(3) Niu, G.; Huang, Y.; Chen, X.; He, J.; Liu, Y.; He, A. Thermal and Hydrothermal Stability of Siliceous Y Zeolite and Its Application to High-Temperature Catalytic Combustion. *Appl. Catal. B* **1999**, *21*, 63.

(4) Gola, A.; Rebours, B.; Milazzo, E.; Lynch, J.; Benazzi, E.; Lacombe, S.; Delevoye L.; Fernandez C. Effect of Leaching Agent in the Dealumination of Stabilized Y Zeolites. *Microporous Mesoporous Mater.* **2000**, *40*, 73.

(5) Zi, G.; Yi, T.; Yugin, Z. Effect of Dealumination Defects on the Properties of Zeolite Y. *Appl. Catal.* **1989**, *56*, 83.

(6) Kugler E. L.; Gardner T. H.; Panpranot, J. Hydrothermal Deactivation Kinetics of FCC Catalysts Containing USY Zeolite. *Abstr. Pap. Am. Chem. Soc.* **1999**, *218*, 34.

(7) Zhdanov, S. P.; Feoktistova, N. N.; Vtjurina, L. M. Temperature Dependence of Nucleation of Zeolites in Alkaline Aluminosilicate Gels in Hydrothermal Crystallization Condition. *Catalysis and Adsorption by Zeolites*; Elsevier Science Publishers B.V.: Amsterdam, 1991; p 287.

(8) Tian, H. P.; Huang, C. J.; Fan, Z. B. Metals on a Novel USY Zeolite after Hydrothermal Aging. *Stud. Surf. Sci. Catal.* **2001**, *139*, 351.

(9) Gutierrez, L.; Boix, A.; Petunchi, J. Promoting Effect of Pt on Co/Zeolites upon the SCR of NO_x. *J. Catal.* **1998**, *179*, 179.

(10) Praserthdam. P.; Phatanasri. S.; Rungsimanop. J.; Kanchanawanichkun. P.; Effect of Pd on the Stability Improvement of Cu/H-MFI for NO Removal under Hydrothermal Pretreatment Condition. *J. Mol. Catal. A: Chem.* **2001**, *169*, 113.

(11) Dangsawai. T.; Praserthdam. P.; Kim. J. B.; Inui. T. Pd Modification of Cu/H−ZSM-5 Catalyst for NO Removal under Hydrothermal Pretreatment Conditions. *Adv. Environ. Res.* **2000**, *3*, 450.

(12) Yang, G.; Wang, Y.; Zhou, J. Q.; Liu, X. C.; Han, X. W.; Bao, X. H. On Configuration of Exchanged La^{3+} in ZSM-5: A Theoretical Approach to the Improvement in Hydrothermal Stability of La-Modified ZSM-5 Zeolite. *J. Chem. Phys.* **2003**, *18*, 9765.

(13) Rajagopalan, K.; Peters, A. W.; Edwards, G. C. Influence of Zeolite Particle size on Selectivity during Fluid Catalytic Cracking. *Appl. Catal.* **1986**, *23*, 69.

(14) Gianetto, A.; Farag, H. I.; Alberto, P. B.; de Lasa, H. I. Fuild Catalytic Cracking Catalyst for Reformulated Gasolines—Kinetic Modeling. *Ind. Eng. Chem. Res.* **1994**, *33*, 3053.

(15) Al-Khattaf, S.; de Lasa, H. The Role of Diffusion in Alkyl-Benzenes Catalytic Cracking. *Appl. Catal. A* **2002**, *226*, 139.

(16) Tatlier, M.; Erdem-Senatalar, A. Optimization of the Cycle Durations of Adsorption Heat Pumps Employing Zeolite Coatings Synthesized on Metal Supports. *Microporous Mesoporous Mater.* **2000**, *34*, 23.

(17) Bonetto, L.; Clamblor, M. A.; Corma, A.; Perez-Pariente, J. Optimization of Zeolite-β in Cracking Catalysts: Influence of Crystallite Size. *Appl. Catal. A.* **1992**, *82*, 37.

(18) Praserthdam, P.; Mongkolsiri, Nakarin.; Kanchanawanichkun, P. Effect of Crystal Size on the Durability of Co/HZSM-5 in Selective Catalytic Reduction of NO by Methane. *Catal Commun.* **2002**, *3*, 191.

(19) Miyanohara, I.; Hashimoto, S.; Miyazaki H. Process for Producing Y-Type Zeolite. U.S. Patent. 4,376,106, 1983.

(20) Linjie, H.; Guofu, X.; Lianglong, Q.; Can, L.; Qin, X.; Dadong, L.; The Effect of Chromium on Sulfur Resistance of Pd/HY−Al_2O_3 Catalysts for Aromatic Hydrogenation. *J. Catal.* **2001**, *202*, 220.

(21) Valtchev, V.; Mintova, S.; Dimov, V.; Toneva, A.; Radev, D. Tribochemical Activation of Seeds for Rapid Crystallization of Zeolite Y. *Zeolites* **1995**, *15*, 193.

(22) Mintova, S.; Valtchev, V.; Vultcheva, E.; Veleva, S. Crystallization Kinetics of Zeolite ZSM-5. *Zeolites* **1992**, *12*, 210.

(23) Cundy, C. S.; Lowe, B. M.; Sinclair, D. M. J. Crystallization of Zeolitic Molecular-Sieves—Direct Measurements of the Growth-Behavior of Single-Crystals as a Function of Synthesis Conditions. *Chem. Faraday Discuss.* **1993**, *95*, 235.

(24) Köroğlu, H. J.; Sarıoğlan, A.; Tather, M.; Şenatalar, A. E.; Savaşç, Ö.T. Effects of Low-Temperature Gel Aging on the Synthesis of Zeolite Y at Different Alkalinities. *J. Crystal Growth* **2002**, *241*, 481.

(25) Gutierrez, L.; Boix, A.; Petunchi, J. Promoting Effect of Pt on Co Zeolites upon the SCR of NO_x. *J. Catal.* **1998**, *179*, 179.

(26) Kubelkova, L.; Seidl, V.; Borbely, G., Beyer, H. K. Correlations between Wavenumbers of Skeletal Vibrations, Unit-Cell Size, and Molar Fraction of Aluminum of Y Zeolites. *J. Chem. Soc., Faraday Trans.* **1988**, *84*(5), 1447.

(27) Aguiar, E. F. S.; Murta Valle, M. L.; Silva, M. P.; Débora, F. S. Influence of External Surface Area of Rare-Earth Containing Y Zeolites on the Cracking of 1,3,5-Triisopropylbenzene. *Zeolites* **1995**, *15*, 620.

(28) Jacobs. P. A. Metal-zeolites: transetters in selective Fischer−Tropsch chemistry. In *Catalysis by zeolites*; Elsevier Science Publishers B.V.: Amsterdam, 1980; p 293.

(29) Di Renzo, F. Zeolites as Tailor-Made Catalysts: Control of the Large Crystal Size. *Catal Today* **1998**, *41*, 37.

(30) Thomas, J. M.; Klinowski, J. The Study of Aluminosilicate and Related Catalysts by High-Resolution Solid-State NMR. *Adv. Catal.* **1985**, *33*, 199.

(31) Budi, P.; Howe, R. F. Steam Deactivation of CoZSM-5 NO_x Reduction Catalysts. *Catal. Today* **1997**, *38*, 175.

(32) Sanz J.; Fornés, V.; Corma, A. Extraframework Aluminum in Steam- and $SiCl_4$-Dealuminated Y Zeolite. *J. Chem, Soc., Faraday Trans.* **1988**, *84*, 3113.

(33) Samoson, A.; Lippmaa, E.; Engelhardt, G.; Lohse, U.; Jerschkewitz, H. G. Quantitative High-Resolution ^{27}Al NMR: Tetrahedral Non-Framework Aluminium in Hydrothermally Treated Zeolites. *Chem. Phys. Lett.* **1987**, *134*, 589.

(34) Omegna, A.; Haouas, M.; Kogelbauer, A.; Prins, R. Realumination of Dealuminated HZSM-5 Zeolites by Acid Treatment: A Reexamination. *Microporous Mesoporous Mater.* **2001**, *46*, 177.

(35) Karge, H. G.; Jozefowicz, L. C. A Comparative Study of the Acidity of Various Zeolites using the Differential Heats of Ammonia Adsorption as Measured by High Vacuum Microcalorimetry. *Stud. Surf. Sci. Catal.* **1994**, *84A*, 685.

(36) Kumar, N.; Nieminen, V.; Dermirkan, K.; Salmi, T.; Murzin, D. Yu.; Laine, E. Effect of Synthesis Time and Mode of Stirring on Physico-Chemical and Catalytic Properties of ZSM-5 Zeolite Catalysts. *Appl. Catal. A* **2002**, *235*, 113.

(37) Satterfield, C. N. *Heterogeneous Catalysis in Industrial Practice*, 2nd ed.; McGraw-Hill: New York, 1991; Vol. 259, p 226.

(38) Falamaki, C.; Edrissi, M.; Sohrabi, M. Studies on the Crystallization Kinetics of Zeolite ZSM-5 with 1,6-Hexanediol as a Structure-Directing Agent. *Zeolites* **1997**, *19*, 362.

Received for review February 25, 2004
Revised manuscript received April 23, 2004
Accepted May 12, 2004

IE049847K

Available online at www.sciencedirect.com
SCIENCE DIRECT®
Journal of Power Sources 142 (2005) 75–80
JOURNAL OF POWER SOURCES
www.elsevier.com/locate/jpowsour

Short communication

Comparison of carbon formation boundary in different modes of solid oxide fuel cells fueled by methane

W. Sangtongkitcharoen[a], S. Assabumrungrat[a,*], V. Pavarajarn[a], N. Laosiripojana[b], P. Praserthdam[a]

[a] *Center of Excellence in Catalysis and Catalytic Reaction Engineering, Department of Chemical Engineering, Chulalongkorn University, Bangkok 10330, Thailand*
[b] *The Joint Graduate School of Energy and Environment, King Mongkut's University of Technology Thonburi, Bangkok 10140, Thailand*

Received 10 August 2004; accepted 20 October 2004
Available online 8 December 2004

Abstract

A detailed thermodynamic analysis is employed as a tool for prediction of carbon formation boundary for solid oxide fuel cells (SOFCs) fueled by methane. Three operating modes of SOFCs, i.e. external reforming (ER), indirect internal reforming (IIR) and direct internal reforming (DIR), are considered. The carbon formation boundary is determined by finding the value of inlet steam/methane (H_2O/CH_4) ratio whose equilibrium gas composition provides the value of carbon activity of one. It was found that the minimum H_2O/CH_4 ratio requirement for which the carbon formation is thermodynamically unfavorable decreases with increasing temperature. For SOFCs with the oxygen-conducting electrolyte, ER-SOFC and IIR-SOFC show the same values of H_2O/CH_4 ratio at the carbon formation boundary, independent of the extent of electrochemical reaction of hydrogen. In contrast, due to the presence of extra H_2O from the electrochemical reaction at the anode chamber, DIR-SOFC can be operated at lower values of the H_2O/CH_4 ratio compared to the other modes. The difference becomes more pronounced at higher values of the extent of electrochemical reaction.

For comparison purpose, SOFCs with the hydrogen-conducting electrolyte were also investigated. According to the study, they were observed to be impractical for use, regarding to the tendency of carbon formation. Higher values of the H_2O/CH_4 ratio are required for the hydrogen-conducting electrolyte, which is mainly due to the difference in location of water formed by the electrochemical reaction at the electrodes. In addition, with this type of electrolyte, the required H_2O/CH_4 ratio is independent on the SOFC operation modes. From the study, DIR-SOFC with the oxygen-conducting electrolyte seems to be the promising choice for operation.

Keywords: Solid oxide fuel cell; Carbon formation; Thermodynamics analysis; Methane

1. Introduction

Solid oxide fuel cell (SOFC) is an energy conversion unit that produces electrical energy and heat with greater energy efficiency and lower pollutant emission than the conventional heat engines, steam and gas turbines, and combined cycles. Due to its high operating temperature, SOFC offers the widest potential range of applications, flexibility of fuel choices and possibility for operation with an internal reformer. Recent developments on SOFCs seem to move towards to two main issues: intermediate temperature operation and use of other fuels instead of hydrogen. The uses of various alternative fuels, i.e. methane, methanol, ethanol, gasoline and other oil derivatives, in SOFCs have been widely investigated [1–3]. To date, methane is a promising fuel as it is an abundant component in natural gas and the methane steam reforming technology is relatively well established. As SOFC is operated at such a high temperature, methane can be reformed effectively by either catalytic steam reforming or partial oxi-

* Corresponding author. Tel.: +662 218 6868; fax: +662 218 6877.
E-mail address: suttichai.a@eng.chula.ac.th (S. Assabumrungrat).

0378-7753/$ – see front matter © 2004 Elsevier B.V. All rights reserved.
doi:10.1016/j.jpowsour.2004.10.009

Nomenclature

a	inlet moles of methane (mol)
b	inlet moles of steam (mol)
c	extent of the electrochemical reaction of hydrogen (mol)
K_1	equilibrium constant of reaction (25) (kPa^{-1})
K_2	equilibrium constant of reaction (26) (kPa)
K_3	equilibrium constant of reaction (27) (kPa^{-1})
n_i	number of moles of component i (mol)
p_i	partial pressure of component i (kPa)
x	converted moles associated with reaction (1) (mol)
y	converted moles associated with reaction (2) (mol)

Subscripts

R	reforming chamber
F	fuel cell chamber

Greek letter

α_c	carbon activity

dation to produce a H_2/CO rich gas, which is eventually used to generate the electrical energy and heat. However, several major problems remain to be solved before such SOFCs can be routinely operated on the direct feed of alternative fuels other than hydrogen. One of them is the problem of carbon deposition on the anode, causing loss of active site and cell performance as well as poor durability. The growth of carbon filaments attached to anode crystallites can generate massive forces within the electrode structure leading to its rapid breakdown [4].

A number of efforts have been carried out to alleviate this problem. One approach is to search for appropriate anode formulations and operating conditions. A number of additives were added to the anode in order to lower the rate of carbon formation. For example, the addition of molybdenum and ceria-based materials to Ni-based anode was reported to reduce carbon deposition, and in some cases, to increase the fuel conversion [5,6]. Addition of alkali, such as potassium, can accelerate the reaction of carbon with steam and also neutralize the acidity of the catalyst support, hence reducing carbon deposition [7].

For the steam reforming, addition of extra steam to the feed is a conventional approach to avoid carbon deposition. Selection of a suitable steam/hydrocarbon ratio becomes an important issue. Carbon formation can occur when the SOFC is operated at low steam/hydrocarbon ratio. However, use of high steam/hydrocarbon ratio is unattractive as it lowers the electrical efficiency of the SOFC by steam dilution of fuel and the system efficiency [6]. Consequently, it is necessary to optimize the suitable steam/hydrocarbon ratio at the carbon formation boundary whose value represents the minimum steam/hydrocarbon ratio required to operate the SOFC at carbon-free condition. Our previous works employed thermodynamic calculations to predict the required steam/alcohol ratio for direct internal reforming SOFCs fed by ethanol [8] and methanol [9]. It was found that the SOFCs with an oxygen-conducting electrolyte require less steam/alcohol ratio than that with a hydrogen-conducting electrolyte because extra steam generated from the electrochemical reaction is available for use in the anode chamber.

In this paper, a detailed thermodynamic analysis is carried out to predict the carbon formation boundary for SOFCs fueled by methane. Three operating modes of SOFCs, i.e. external reforming (ER), indirect internal reforming (IIR) and direct internal reforming (DIR), with two electrolyte types, i.e. oxygen- and hydrogen-conducting electrolytes, are investigated to compare the required steam/methane (H_2O/CH_4) ratios between different SOFC operating modes.

2. Theory

The main reactions involved in the production of hydrogen from methane and water are the methane steam reforming and water gas shift reactions as shown in Eqs. (1) and (2), respectively.

$$CH_4 + H_2O = 3H_2 + CO \quad (1)$$

$$CO + H_2O = H_2 + CO_2 \quad (2)$$

The former is strongly endothermic while the latter is mildly exothermic. Methane steam reforming is commercially operated at 1000–1100 K and 2.17–2.86 MPa over nickel based catalysts [10]. The feed contains steam in excess of the stoichiometric amount with H_2O/CH_4 molar ratios of 3–5 to prevent soot formation [11].

When SOFCs are operated with a fuel, such as hydrocarbon and alcohol, three modes of operation, i.e. external reforming SOFC (ER-SOFC), indirect internal reforming SOFC (IIR-SOFC) and direct internal reforming SOFC (DIR-SOFC) as shown in Fig. 1, are possible. For ER-SOFC operation, the endothermic steam reforming and the electrochemical reactions are operated separately in different units, and there is no direct heat transfer between both units. High energy supply to the outside reformer is required due to the high endothermic over this part. In contrast, for both IIR-SOFC and DIR-SOFC, the endothermic reaction from the steam reforming reaction and the exothermic reaction from the oxidation reaction are operated together in a single unit. Therefore, the requirement of a separate fuel reformer and energy supply to this unit can be eliminated. This configuration is expected to simplify the overall system design, making SOFC more attractive and efficient means of producing electrical power.

For IIR-SOFC, the reforming reaction occurs in the vicinity of the cell stack. This enables heat transfer from the fuel

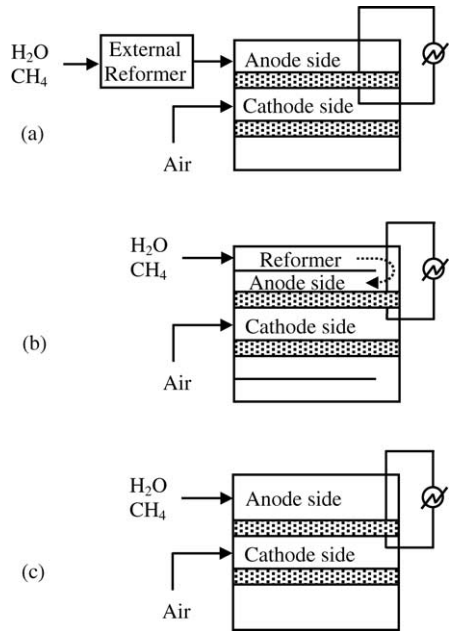

Fig. 1. Configurations of various SOFC modes. (a) ER-SOFC, (b) IIR-SOFC and (c) DIR-SOFC.

cell chamber to the reformer, which leads to energetic economy. However, part of heat may not be efficiently utilized due to its limited heat transfer rate. For DIR operation, the reforming reaction takes place at the anode of the fuel cell. Heat and steam released from the electrochemical reaction upon power generation is effectively used for the endothermic reforming reaction since both processes take place simultaneously at the anode. Therefore, in term of energy aspect, DIR-SOFC is more attractive than the others. It should be noted that state-of-the-art SOFC nickel cermet anodes can provide sufficient activity for the steam reforming and shift reactions without the need for additional catalysts [4,12].

Two types of solid electrolytes can be employed in the SOFC, i.e. oxygen- and hydrogen-conducting electrolytes. The reactions taking place in the anode and the cathode can be summarized as follows:

- Oxygen-conduction electrolyte:

$$\text{anode}: \quad H_2 + O^{2-} = H_2O + 2e^- \tag{3}$$

$$\text{cathode}: \quad O_2 + 4e^- = 2O^{2-} \tag{4}$$

- Hydrogen-conducting electrolyte:

$$\text{anode}: \quad H_2 = 2H^+ + 2e^- \tag{5}$$

$$\text{cathode}: \quad 2H^+ + \tfrac{1}{2}O_2 + 2e^- = H_2O \tag{6}$$

The difference between both electrolyte types is the location of the water produced. With the oxygen-conducting electrolyte, water is produced in the reaction mixture in the anode chamber. In the case of the hydrogen-conducting electrolyte, water appears on the cathode side. The number of moles of each component involved in different SOFC modes is discussed in the following sections.

2.1. ER-SOFC and IIR-SOFC

For ER-SOFC and IIR-SOFC, the methane steam reforming and water gas shift reaction take place initially at the reforming chamber. Then the exit gas from the reformer is fed to the fuel cell chamber where all the methane steam reforming, water gas shift reaction and electrochemical reactions occur. If required, additional water feed can be added to the reformer exit gas before being fed to the fuel cell chamber. The number of moles of each component is given by the following expressions:

- Reforming chamber

$$n_{CH_4} = a - x_R \tag{7}$$

$$n_{CO} = x_R - y_R \tag{8}$$

$$n_{CO_2} = y_R \tag{9}$$

$$n_{H_2} = 3x_R + y_R \tag{10}$$

$$n_{H_2O} = b_R - x_R - y_R \tag{11}$$

$$n_{total} = \sum_{i-1}^{5} n_i \tag{12}$$

where a and b_R represent the inlet moles of methane and water, respectively, and x_R and y_R are the converted moles in the reforming chamber associated to the reactions (1) and (2), respectively.

- Fuel cell chamber

$$n_{CH_4} = a - x_R - x_F \tag{13}$$

$$n_{CO} = x_R - y_R + x_F - y_F \tag{14}$$

$$n_{CO_2} = y_R + y_F \tag{15}$$

$$n_{H_2} = 3x_R + y_R + 3x_F + y_F - c \tag{16}$$

$$\begin{aligned} n_{H_2O} &= b_R - x_R - y_R + b_F - x_F - y_F \\ &\quad \text{(for hydrogen-conducting electrolyte)} \\ n_{H_2O} &= b_R - x_R - y_R + b_F - x_F - y_F + c \\ &\quad \text{(for oxygen-conducting electrolyte)} \end{aligned} \tag{17}$$

$$n_{total} = \sum_{i-1}^{5} n_i \tag{18}$$

where b_F is the additional mole of water fed to the fuel cell chamber, x_F and y_F the converted moles in the fuel cell chamber associated to the reactions (1) and (2), respectively and c is the extent of the electrochemical reaction of hydrogen. It should be noted that only hydrogen is assumed to react electrochemically with oxygen supplied from the cathode side. Then, the overall inlet H_2O/CH_4 ratio for these modes is equal to $(b_R + b_F)/a$.

2.2. DIR-SOFC

For DIR-SOFC, as described, there is no requirement of the separated reforming chamber in the system. All the reactions mentioned earlier take place simultaneously in the fuel cell chamber. The number of moles of each component is given by the following expressions:

$$n_{CH_4} = a - x_F \tag{19}$$

$$n_{CO} = x_F - y_F \tag{20}$$

$$n_{CO_2} = y_F \tag{21}$$

$$n_{H_2} = 3x_F + y_F - c \tag{22}$$

$$\begin{aligned} n_{H_2O} &= b_F - x_F - y_F + c \\ &\quad \text{(for oxygen-conducting electrolyte)} \\ n_{H_2O} &= b_F - x_F - y_F \\ &\quad \text{(for hydrogen-conducting electrolyte)} \end{aligned} \tag{23}$$

$$n_{total} = \sum_{i-1}^{5} n_i \tag{24}$$

Calculations of the thermodynamic equilibrium composition are accomplished by solving a system of non-linear equations relating the moles of each component to the equilibrium constants of the reactions.

The following reactions are the most probable reactions that lead to carbon formation in the reaction system [13]:

$$2CO = CO_2 + C \tag{25}$$

$$CH_4 = 2H_2 + C \tag{26}$$

$$CO + H_2 = H_2O + C \tag{27}$$

The Boudard reaction (Eq. (25)) and the decomposition of methane (Eq. (26)) are the major pathways for carbon formation at high operating temperature [14]. It should be noted that due to the exothermic nature of the water gas shift reaction (Eq. (2)), the amount of CO becomes significant at high temperature [15]. All reactions are employed to examine the thermodynamic possibility of carbon formation. The carbon activities, defined in Eqs. (28)–(30), are used to determine the possibility of carbon formation.

$$\alpha_{c,CO} = K_1 \frac{p_{CO}^2}{p_{CO_2}} \tag{28}$$

$$\alpha_{c,CH_4} = K_2 \frac{p_{CH_4}}{p_{H_2}{}^2} \tag{29}$$

$$\alpha_{c,CO-H_2} = K_3 \frac{p_{CO} p_{H_2}}{p_{H_2O}} \tag{30}$$

where K_1, K_2 and K_3 represent the equilibrium constants of the reactions (25), (26) and (27), respectively, and p_i is the partial pressure of component i. When $\alpha_c > 1$, the system is not in equilibrium and carbon formation is observed. The system is at equilibrium when $\alpha_c = 1$. It is noted that the carbon activity is only the indicator for the presence of carbon in the system. It does not give the information regarding the amount of carbon formed. Finally, when $\alpha_c < 1$, carbon formation is thermodynamically impossible.

In order to identify the range of SOFC operation, which does not suffer from the formation of carbon, the operating temperature and the extent of the electrochemical reaction of hydrogen are specified. Then the initial value of the H_2O/CH_4 ratio is varied and the corresponding values of α_c are calculated. The carbon formation boundary is defined as the value of H_2O/CH_4 whose value of $(1-\alpha_c)$ is approaching zero. This value represents the minimum inlet H_2O/CH_4 mole ratio at which carbon formation in the equilibrium mixture is thermodynamically impossible. For ER-SOFC and IIR-SOFC, the calculations for both reformer and fuel cell chambers are required. It should be noted that although recent investigators estimated the carbon concentration in the steam reforming reactions by the method of Gibbs energy minimization, the principle of equilibrated gas to predict the carbon formation in this study is still meaningful because the calculations are carried in order to determine the carbon formation boundary where the carbon starts forming on the surface. In addition, other possible factors such as mass and heat transfer or rate of reactions may also affect the prediction of the carbon formation boundary. Local compositions, which allow the local carbon formation, may exist although the carbon formation is unfavorable according to the calculation based on equilibrium bulk compositions. Moreover, other forms of carbonaceous compounds such as C_nH_m may be formed and result in comparable damages.

3. Results and discussion

The influence of inlet steam/methane (H_2O/CH_4) ratio on equilibrium composition of species at the reformer section was firstly carried out as illustrated in Fig. 2. The molar fractions of CO_2, H_2O and H_2 increased with increasing the inlet steam/methane ratio, whereas the decrease in CO production

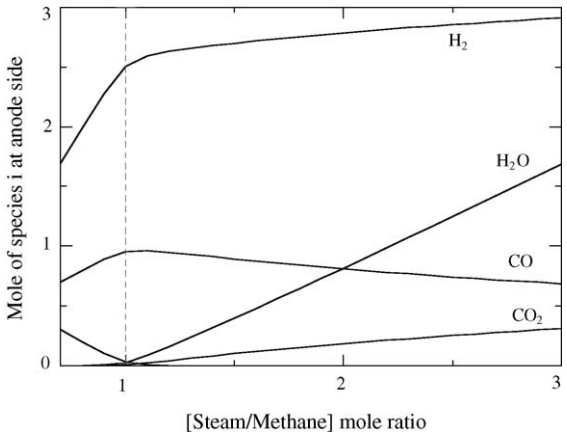

Fig. 2. Effect of inlet H_2O/CH_4 ratio on each component mole in the reformer (a = 1 mol, P = 101.3 kPa and T = 1173 K).

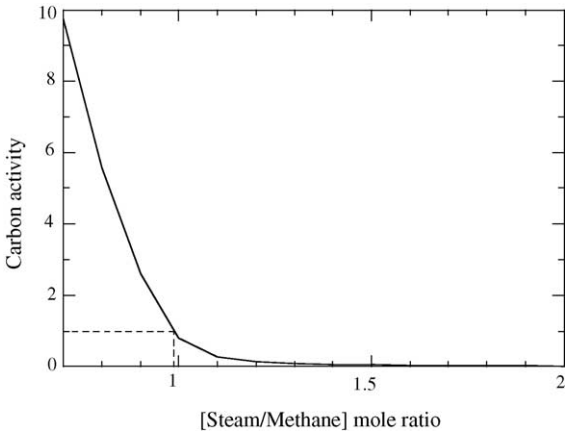

Fig. 3. Effect of inlet H_2O/CH_4 ratio on carbon activity in the reformer (a = 1 mol, P = 101.3 kPa and T = 1173 K).

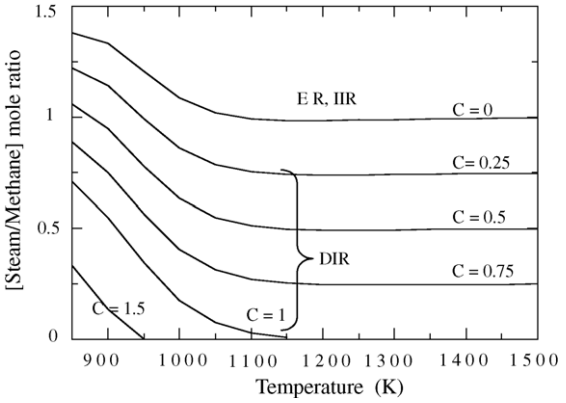

Fig. 4. Influence of the operation mode on the requirement of inlet H_2O/CH_4 ratio at different operating temperatures (oxygen-conducting electrolyte, a = 1 mol and P = 101.3 kPa).

is observed. Apparently, the increasing of inlet H_2O/CH_4 ratio moves both methane steam reforming (Eq. (1)) and water gas shift reaction (Eq. (2)) into the forward direction. The number of mole for methane is very small since it is the reactant of the endothermic reaction, which proceeds in great extent at high temperature. It should be noted that according to Eqs. (25)–(27), the presence of high molar fractions of CO_2, H_2 and H_2O is effective for preventing the carbon formation in the system.

Fig. 3 shows the influence of inlet H_2O/CH_4 ratio on the corresponding values of the carbon activity calculated from the equilibrium compositions. The initial high slope at the low H_2O/CH_4 ratio implies that the opportunity of the carbon formation is rapidly decreased with an addition of steam into the system. The carbon formation becomes thermodynamically unfavored, as the carbon activity is less than one, when the H_2O/CH_4 ratio is approximately greater than one. It is therefore indicated that the carbon formation is less likely as the H_2O/CH_4 ratio is increased. It should also be noted that the values of carbon activities calculated from Eqs. (28)–(30) are equal because the calculations are based on the gas phase compositions at equilibrium. This is also observed by other investigator [16].

Fig. 4 shows the H_2O/CH_4 ratio at the carbon formation boundary for typical SOFCs with the oxygen-conducting electrolyte for different operating modes and various extents of electrochemical reaction of hydrogen. It can be seen from the figure that the required inlet H_2O/CH_4 ratio for avoiding carbon formation decreases with increasing operating temperature and becomes constant at high temperature. This similar behavior was reported in our previous works with other types of fuel including ethanol [8] and methanol [9]. Therefore, raising the SOFC operating temperature is one possibility to prevent carbon formation at the anode, however, the cost of high temperature materials as well as the problem of cell sealing must also be considered. Comparison between different operating modes indicates that the required H_2O/CH_4 ratios for ER-SOFC and IIR-SOFC are the same, independent of the extent of electrochemical reaction of hydrogen. In contrast, for DIR-SOFC, hydrogen from the electrochemical reaction is converted to steam at the anode side, where the reforming reaction simultaneously takes place and, consequently reduces the requirement of H_2O/CH_4 ratio in the feed. It is particularly pronounced when DIR-SOFC is operated at high current density. Nevertheless, due to the fact that DIR-SOFC requires anode material with sufficient catalytic activity for both reforming and electrochemical reactions whereas ER-SOFC and IIR-SOFC can employ two separated materials readily available for each reaction, ER-SOFC and IIR-SOFC may be preferred at the moment. In case that either ER-SOFC or IIR-SOFC with the oxygen-conducting electrolyte is employed, it should be noted that the damage from carbon deposition in the fuel cell chamber would be less likely, comparing to that in the reformer. Water produced from the electrochemical reaction in the fuel cell chamber in addition to the amount of water in the inlet stream, which is already adjusted to avoid the formation of carbon in the reformer, further decreases the possibility of carbon deposition in the fuel cell chamber.

For comparison, the requirement of H_2O/CH_4 ratios to prevent the carbon formation for ER-SOFC, IIR-SOFC, and DIR-SOFC with the hydrogen-conducting electrolyte are also carried out as shown in Fig. 5. Independent of the operating modes, more inlet steam is required when the cell is operated at high extents of electrochemical reaction of hydrogen. It should be noted that the benefit of steam generation at the cathode by the electrochemical reaction is not recognized for this system. The disappearance of hydrogen from the anode side by electrochemical reaction favors the carbon formation and, consequently required higher steam in order to prevent the formation of carbon species.

From the above results, DIR-SOFC with the oxygen-conducting electrolyte seems to be a promising operation mode due to the good heat utilization within the system and the reduction of inlet H_2O/CH_4 ratio requirement. This summary is in contrast to one previous work, which reported that the SOFC with the hydrogen-conducting electrolyte provides higher electrical efficiency than that with the oxygen-

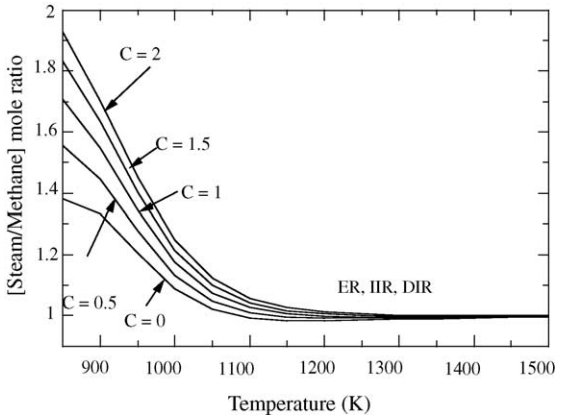

Fig. 5. Influence of operation mode on the requirement of inlet H_2O/CH_4 ratio at different operating temperatures (hydrogen-conducting electrolyte, $a = 1$ mol and $P = 101.3$ kPa).

conducting electrolyte because high partial of hydrogen is maintained at the anode side [17]. However, since the comparison in that work was based on the calculations using the same value of inlet H_2O/CH_4 ratio, the benefit from the reduced steam requirement was not taken into account. This subject will be discussed in more details in our next paper dealing with the efficiency of the overall SOFC system.

4. Conclusion

Theoretical thermodynamic analysis was performed to predict the carbon formation boundary for the SOFCs with different operating modes. It was observed that the required H_2O/CH_4 ratio to prevent the carbon formation mainly depended on the operating temperature, SOFC operation mode, and electrolyte type. In general, operation at high temperature reduces the required inlet H_2O/CH_4 ratio in all cases. The oxygen-conducting electrolyte is more attractive than the hydrogen-conducting electrolyte as the former system requires less steam. This is directly related to water generated from the electrochemical reaction of hydrogen at electrodes. The difference in steam requirement is particularly pronounced at high extent of the electrochemical reaction of hydrogen. The required H_2O/CH_4 ratio is independent of the SOFC operating modes for those with the hydrogen-conducting electrolyte. On the other hand, for the SOFC with the oxygen-conducting electrolyte, DIR-SOFC requires less steam than both ER-SOFC and IIR-SOFC. In summary, the DIR-SOFC with the oxygen-conducting electrolyte seems to be a favorable choice for SOFC operation in the point of view of the amount of steam required.

It should be noted that although the thermodynamic calculations can be used to predict the minimum inlet H_2O/CH_4 ratio for which carbon formation is not favored, the deactivation of anode is not solely the result from the deposition of carbon. Deposition of other forms of carbonaceous compounds such as polymeric coke (C_nH_m) may result in comparable damage. Therefore, the results obtained in this study should be considered only as crude guideline for operating condition of SOFC.

Acknowledgement

The supports from the Thailand Research Fund and the Chulalongkorn University Graduate Scholarship commemoratory the 7th Anniversary of H.M. King Rama IX, and suggestions from Professor Jaime Wisniak are gratefully acknowledged.

References

[1] S.L. Douvartzides, F.A. Coutelieris, K. Demin, P.E. Tsiakaras, AIChE J. 49 (2003) 248–257.
[2] L.F. Brown, Int. J. Hydrogen Energy 26 (2001) 381–397.
[3] G. Maggio, S. Freni, S. Cavallaro, J. Power Sources 74 (1998) 17–23.
[4] S.H. Clarke, A.L. Dicks, K. Pointon, T.A. Smith, A. Swann, Catal. Today 38 (1997) 411–423.
[5] C.M. Finnerty, R.M. Ormerod, J. Power Sources 86 (2000) 390–394.
[6] S. Park, R.J. Gorte, J.M. Vohs, Appl. Catal. A 200 (2000) 55–61.
[7] C.M. Finnerty, N.J. Coe, R.H. Cunningham, R.M. Ormerod, Catal. Today 46 (1998) 137–145.
[8] S. Assabumrungrat, V. Pavarajarn, S. Charojrochkul, N. Laosiripojana, Chem. Eng. Sci. 59 (2004) 6017–6022.
[9] S. Assabumrungrat, N. Laosiripojana, V. Pavarajarn, W. Sangtongkitcharoen, A. Tangjitmatee, P. Praserthdam, J. Power Sources 139 (2005) 55–60.
[10] T.A. Czuppon, S.A. Knez, D.A. Newsome, Hydrogen, in: J.L. Kroschwitz, M. Howe-Grant (Eds.), Kirk-Othmer, Encyclopedia of Chemical Technology, vol. 13, fourth ed., Wiley, New York, 1995, pp. 383–394, esp. 852–865.
[11] H.-J. Renner, F. Marschner, Catalytic reforming of natural gas and other hydrocarbon, in: B. Elvers, S. Hawkins, M. Ravenscroft, J.F. Rousaville, G. Schulz (Eds.), Ullmann's Encyclopedia of Industrial Chemistry, vol. A2, fifth ed., VCH Verlagsgesellschaft, Weinheim, Germany, 1985, pp. 143-242, esp. 186–204.
[12] A.L. Dicks, J. Power Sources 717 (1998) 111–122.
[13] P. Pietrogrande, M. Bezzeccheri, in: L.J.M.J. Blomen, M.N. Mugerwa (Eds.), Fuel Cell Systems, Plenum Press, New York, 1993, p. 142.
[14] J.N. Amor, Appl. Catal. A 176 (1999) 159–176.
[15] L.F. Brown, Int. J. Hydrogen Energy 26 (2001) 381–397.
[16] S. Nagata, A. Momma, T. Kato, Y. Kasuga, J. Power Sources 101 (2001) 60–71.
[17] A.K. Demin, P.E. Tsiakaras, V.A. Sobyanin, S.Y. Hramova, Solid State Ionics 152–153 (2002) 555–560.

Available online at www.sciencedirect.com
SCIENCE DIRECT®
Materials Chemistry and Physics 89 (2005) 395–401
MATERIALS CHEMISTRY AND PHYSICS
www.elsevier.com/locate/matchemphys

Dependence of crystalline phases in titania on catalytic properties during CO hydrogenation of Co/TiO_2 catalysts

Bunjerd Jongsomjit*, Chitlada Sakdamnuson, Piyasan Praserthdam

Department of Chemical Engineering, Faculty of Engineering, Center of Excellence on Catalysis and Catalytic Reaction Engineering, Chulalongkorn University, Bangkok 10330, Thailand

Received 20 July 2004; received in revised form 7 September 2004; accepted 20 September 2004

Abstract

The present research showed dependence of crystalline phases in titania on the catalytic properties of Co/TiO_2 catalysts during CO hydrogenation. A comparative study of anatase TiO_2- and rultile-anatase coupled TiO_2-supported Co catalysts was conducted. It was found that the presence of rutile phase (19 mol%) in titania resulted in a significant increase in the catalytic activity during CO hydrogenation. It was proposed that the role of rutile phase was to increase the stability of the support. The impact of water vapor produced during reduction on the formation of cobalt species strongly interacted with the support was probably inhibited by the presence of rutile phase in titania leading to a decrease in the reducibility loss during reduction.

Keywords: Supported catalyst; Cobalt catalyst; CO hydrogenation; Titania; Reducibility

1. Introduction

In Fischer–Tropsch (FT) catalysis, supported cobalt (Co) catalysts are preferred because of their high activities during FT synthesis based on natural gas [1], high selectivity to linear long chain hydrocarbons and also low activities for the competitive water–gas shift (WGS) reaction [2,3]. Many inorganic supports such as SiO_2 [4–8], Al_2O_3 [9–14], TiO_2 [15–17] and Zeolites [18] have been extensively studied for supported Co catalysts for years. It is known that in general, the catalytic properties depend on reaction conditions, catalyst compositions, metal dispersion, and types of inorganic supports used. Thus, changes the catalyst compositions and/or even though the compositions of supports used may lead to significantly enhance the catalytic properties as well.

During the past decade, titania-supported Co catalysts have been widely investigated by many authors, especially for the application of FT synthesis in a continuously stirred tank reactor (CSTR) [15–17]. However, it should be noted that titania itself has different crystalline phases such as anatase and rutile phases. The different crystalline phase compositions of titania could play an important role on the catalytic performance of titania-supported Co catalysts during CO hydrogenation as well. Thus, the main objective of this research was to investigate influences of different crystalline phases of titania supports on the catalytic properties during CO hydrogenation of Co/TiO_2 catalysts. In the present study, the Co/TiO_2 catalysts were prepared using different crystalline phase compositions of titania supports. The catalysts were pretreated, characterized and tested in order to evaluate the catalytic properties during CO hydrogenation.

2. Experimental

2.1. Catalyst preparation

A 20 wt.% of Co/TiO_2 was prepared by the incipient wetness impregnation. A designed amount of cobalt nitrate [$Co(NO_3)\cdot 6H_2O$] was dissolved in deionized water and then impregnated onto TiO_2 (contained 100 mol% of anatase phase calcined at 500 °C, obtained from Ishihara Sangyo, Japan) and onto TiO_2 (contained 81 mol% of anatase phase

* Corresponding author. Tel.: +66 2 2186869; fax: +66 2 2186877.
E-mail address: bunjerd.j@chula.ac.th (B. Jongsomjit).

0254-0584/$ – see front matter © 2004 Elsevier B.V. All rights reserved.
doi:10.1016/j.matchemphys.2004.09.019

and 19 mol% of rutile phase, also obtained from Ishihara Sangyo, Japan). The catalyst precursor was dried at 110 °C for 12 h and calcined in air at 500 °C for 4 h.

2.2. Catalyst pretreatments

2.2.1. Standard reduction

Standard reduction of the calcined catalyst was conducted in a fixed-bed flow reactor under differential conditions at 1 atm using a temperature ramp from ambient to 350 °C at 1 °C min^{-1} and holding at 350 °C for 10 h in a gas flow having a space velocity of 16,000 h^{-1} and consisting of H_2. The high space velocity of the H_2 flow was applied to insure that the partial pressure of water vapor in the catalyst bed produced by cobalt oxide reduction would be essentially zero. The reduced catalyst was then passivated at room temperature with air for 30 min prior to taking it out.

2.2.2. Hydrothermal treatment

In order to evaluate the stability of catalysts and impacts of water vapor during reduction, hydrothermal treatment was also conducted during standard reduction above. In addition, besides using pure H_2, mixtures of H_2 and water vapor (5–10 vol.%) were also applied separately at the same reduction condition as mentioned in Section 2.2.1.

2.3. Catalyst nomenclature

The nomenclature used for the catalyst samples in this study is as follows:

- Co/T1: titania (100 mol% of anatase phase)-supported Co catalyst;
- Co/T2: titania (81 mol% of anatase phase and 19 mol% of rutile phase)-supported Co catalyst;
- (C): calcined catalyst sample;
- (RW0), (RW5) and (RW10): reduced catalyst samples with no water vapor, 5 vol.% of water vapor, and 10 vol.% of water vapor, added during standard reduction, respectively.

2.4. Catalyst characterization

2.4.1. BET surface area

BET surface area of the samples after various pretreatments was performed to determine if the total surface area changes upon the various pretreatment conditions. It was determined using N_2 adsorption at 77 K in a Micromeritics ASAP 2010.

2.4.2. X-ray diffraction

XRD was performed to determine the bulk crystalline phases of catalyst following different pretreatment conditions. It was conducted using a SIEMENS D-5000 X-ray diffractometer with Cu Kα (λ = 1.54439 Å). The spectra were scanned at a rate of 2.4° min^{-1} in the range 2θ = 20–80°.

2.4.3. Scanning electron microscopy and energy dispersive X-ray spectroscopy

SEM and EDX were used to determine the catalyst morphologies and elemental distribution throughout the catalyst granules, respectively. The SEM of JEOL mode JSM-5800LV was applied. EDX was performed using Link Isis series 300 program.

2.4.4. Raman spectroscopy

The Raman spectra of the samples were collected by projecting a continuous wave laser of argon ion (Ar^+) green (514.532 nm) through the samples exposed to air at room temperature. A scanning range of 100 to 1000 cm^{-1} with a resolution of 2 cm^{-1} was applied. The data were analyzed using the Renishaw WiRE (Windows-based Raman Environment) software, which allows Raman spectra to be captured, calibrated, and analyzed using system 2000 functionality via Galactic GRAMS interface with global imaging capacity.

2.4.5. Temperature-programmed reduction

TPR was used to determine the reduction behaviors and reducibilities of the samples. It was carried out using 50 mg of a sample and a temperature ramp from 35 to 800 °C at 5 °C min^{-1}. The carrier gas was 5% H_2 in Ar. A cold trap was placed before the detector to remove water produced during the reaction. A thermal conductivity detector (TCD) was used to determine the amount of H_2 consumed during TPR. The H_2 consumption was calibrated using TPR of Ag_2O at the same conditions. The reduced samples were recalcined at the original calcination conditions prior to performing TPR. The calculation of reducibilities was described in elsewhere [9,19–22].

2.5. Reaction

CO hydrogenation (H_2/CO = 10/1) was performed to determine the overall activity of the catalyst samples reduced at various conditions. Hydrogenation of CO was carried out at 220 °C and 1 atm. A flow rate of H_2/CO/He = 20/2/8 cc min^{-1} in a fixed-bed flow reactor under differential conditions was used. A relatively high H_2/CO ratio was used to minimize deactivation due to carbon deposition during reaction. Typically, 20 mg of a catalyst sample was re-reduced in situ in flowing H_2 (30 cc min^{-1}) at 350 °C for 10 h prior to the reaction. Reactor effluent samples were taken at 1 h intervals and analyzed by GC. In all cases, steady-state was reached within 5 h.

3. Results and discussion

The present study was conducted in order to investigate the dependence of crystalline phases in titania on the catalytic properties during CO hydrogenation of Co/TiO_2 catalysts. As mentioned, in general titania used contains mainly two phases; anatase and rutile phases. Phase transfor-

mation of titania depends on the preparation of titania such as sol–gel or solvothermal methods and also calcination temperatures. However, it was proposed that the different phase compositions in titania could play an important role on the catalytic properties during CO hydrogenation of Co/TiO_2 catalysts. Section 3 is divided into two parts as follows:

3.1. Catalyst stability during reduction under hydrothermal treatments

It is known that Co metal rather than its oxide or carbide is the active form of supported Co catalysts during CO hydrogenation. Thus, reduction of Co oxide precursor is required in order to reduce it into Co metal form. Water vapor is a byproduct of reduction of metal oxide. It is also known that water vapor also has impacts on the reduction of alumina-supported Co oxide probably in two ways: (i) facilitation of the migration of Co ions into tetrahedral sites of alumina to form a non-reducible (at temperatures <900 °C) spinel; and (ii) inhibition of well-dispersed CoO interacting with the alumina support, posssibly by increasing the cobalt–alumina interaction [22]. Moreover, Co-Support compound formation (Co-SCF) can be formed during reduction, especially, when alumina [19] and silica [21] are used as the supports for Co catalysts. Thus, in order to evaluate the impacts of water vapor on the stability of Co/TiO_2 catalysts, hydrothermal treatments during reduction of the catalysts was also performed. After various pretreatments, the catalysts were characterized using different techniques. XRD patterns of samples are shown in Fig. 1. It can be observed that the T1 support contained pure anatase TiO_2, whereas the T2 support is composed of rutile (19 mol%) and anatase (81 mol%) forms. XRD patterns of T1 showed strong diffraction peaks at 26, 37, 48, 55, 62, 69, 71 and 75° indicating the TiO_2 in its anatase form. The additional diffraction peaks at 27, 36, 42 and 57° can been seen in XRD patterns of the T2 support indicating the presence of rutile phase in titania. The cobalt species on both supports exhibited the similar XRD patterns regardless of the pretreatment conditions. As expected, Co_3O_4 were detected at 36, 46 and 65° after calcination of samples. However, after reduction and passivation, only diffraction peaks at 37 and 63° corresponding to CoO were observed. Basically, after reduction of the calcined samples, Co_3O_4 species was reduced to Co^0 metal. However, after passivation with air, thin layer of CoO species was formed at the catalyst surface to prevent rapid oxidation by Co^0 metal when exposed to air as also reported [19,20]. As mentioned above, Co^0 metal was formed after reduction. However, Co^0 was present in a highly dispersed form, thus, invisible by XRD. The similar results were also reported [19,20]. Reduction process is conducted in order to transform Co-oxide species into the active Co^0 metal for catalyzing CO hydrogenation. Raman spectra of all pretreated samples are shown in Fig. 2. The similar trend in Raman spectroscopy was also observed as seen for XRD results. It was found that T1 support exhibited Raman bands

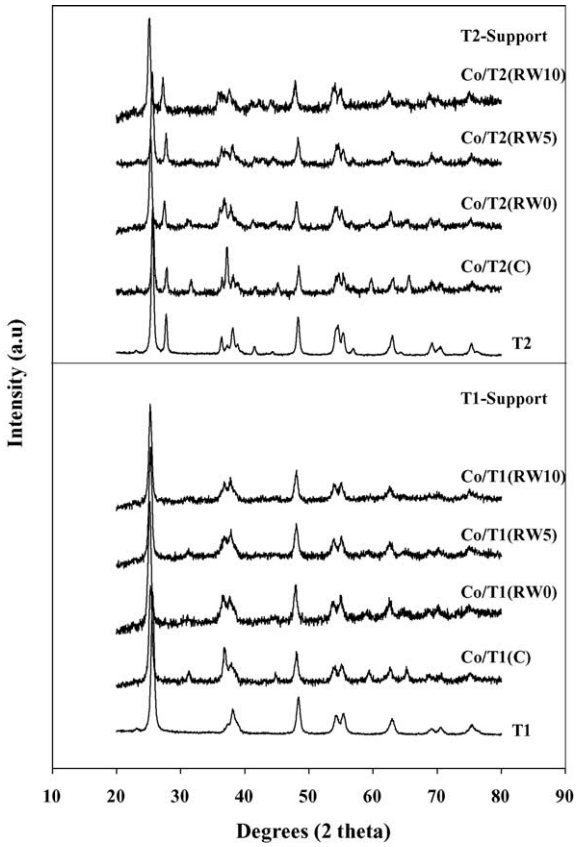

Fig. 1. XRD patterns of T1 and T2 supports, and catalyst samples pretreated under various conditions.

at 640, 514 and 397 cm^{-1} for TiO_2 in its anatase form. Besides the identical Raman bands as shown for the T1 support, the T2 support additionally exhibited a shoulder band around 445 cm^{-1} indicating TiO_2 in its rutile form. The Raman spectra for calcined samples in both T1 and T2 supports exhibited similar Raman bands at 640, 514 and 397 cm^{-1} as seen in those for T1 and T2 supports solely including two shoulders at 690 and 480 cm^{-1}, assigned to Co_3O_4 [9,19,20]. Raman spectra of all reduced samples showed the Raman bands of titania (T1 or T2) and the shoulders at 690 and 480 cm^{-1}. These can be assigned to Co_3O_4 present on catalyst surface rather than CoO (detected in the bulk by XRD) since Raman spectroscopy is more of surface technique [20]. SEM and EDX were also performed in order to study the morphologies and elemental distributions of catalyst after various pretreatments. However, no significant changes in morphologies and elemental distributions (not shown) were observed upon various pretreatment conditions used in this study. In summary, it should be noted that upon the various pretreatments even with or without hydrothermal treatments, the cobalt species on both T1 and T2 supports, essentially, exhibited the similar characteristics detected by XRD, Raman spectroscopy, and SEM/EDX. No surface compound species between Co and titania, if present, can be detected using those above techniques.

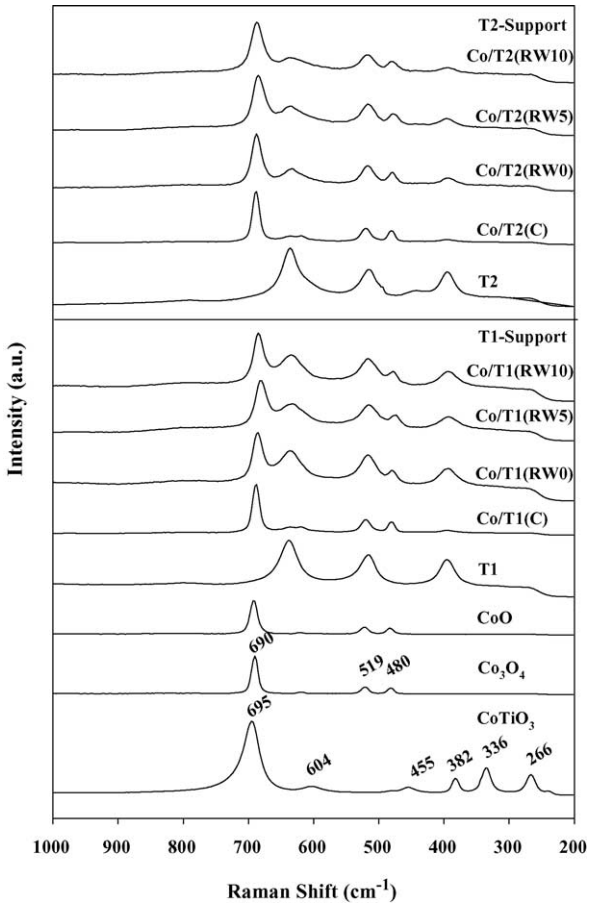

Fig. 2. Raman spectra of T1 and T2 supports, CoO, Co_3O_4, $CoTiO_3$, and catalyst samples pretreated under various conditions.

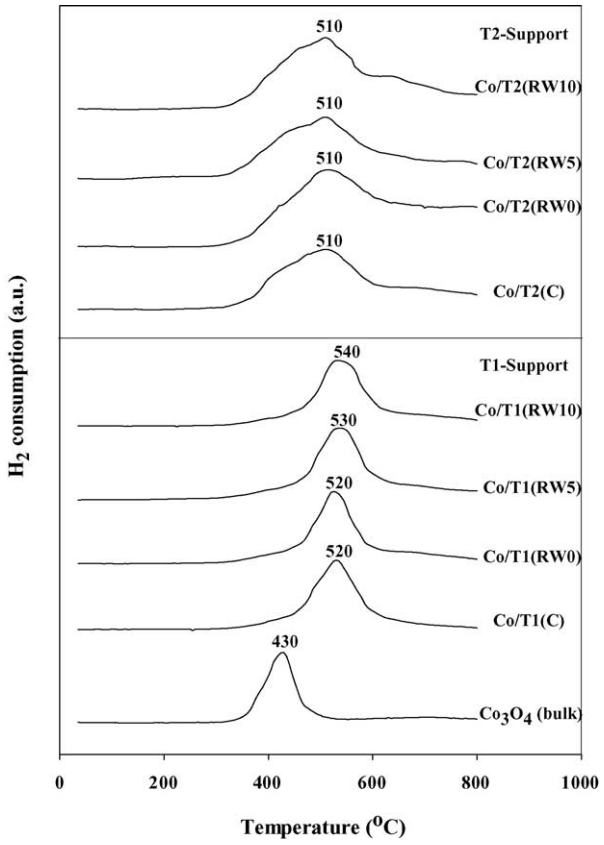

Fig. 3. TPR profiles of catalyst samples pretreated under various conditions.

TPR was performed to study reduction behaviors and to measure reducibility of catalysts. TPR profiles of all samples and Co_3O_4 are shown in Fig. 3. It was found that TPR profile of titania supports (not shown) for both T1 and T2 supports exhibited no reduction peak at this TPR condition. Only one strong reduction peak (max. at 430 °C) can be observed for bulk Co_3O_4 assigned to the overlap of two-step reduction of Co_3O_4 to CoO and then to Co^0 [22–24]. Upon the TPR conditions, the two-step reduction may or may not be observed. For T1 support, only one reduction peak located at ca. 370–620 °C (max. at 520 °C) can be observed for the calcined sample (Co/T1-C) indicated that no residual cobalt nitrates remain on the calcined samples upon calcination condition used in this study. TPR profiles for all reduced samples with T1 support were also similar exhibiting only one reduction peak located at ca. 400–620 °C. The maximum temperature at ca. 520 °C for Co/T1-RW0 was shifted about 10 and 20 °C when hydrothermal treatment was performed during reduction as seen for Co/T1-RW5 and Co/T1-RW10 samples, respectively. The shift of a reduction peak to a higher temperature (ca. 10–20 °C) indicates stronger interaction between cobalt and titania support. It is known that the amounts of Co species strongly interacted with the support are also proportional to the partial pressure of water vapor present during reduction [9,19–22]. For the T2 support, all pretreated samples also exhibited only one reduction peak (max. at 510 °C). However, it should be mentioned that there was no significant shift of the reduction temperatures upon the hydrothermal treatment during reduction indicating a lesser degree of cobalt-support interaction compared to what we have seen for the cobalt species on the T1 support. It was suggested that the presence of rutile phase (19 mol%) in T2 should result in an increase in stability of the titania support even though hydrothermal treatment was applied during reduction. An increase in stability of T2 support could be the cause for a difficulty of cobalt to interact with it.

Besides reduction behaviors obtained from TPR results, reducibilities of samples can be measured based on the peak areas below TPR curve (calibrated using Ag_2O), which are related to the amounts of hydrogen consumed during TPR [9,19–22]. The calculated reducibilities along with the BET surface areas of samples are shown in Table 1. There was no significant change in surface areas upon the pretreatment conditions used in this study. It was observed that for both T1 and T2 supports, the reducibilities decreased when the calcined samples were reduced and performed TPR indicating a loss in reducibility of cobalt oxide species after reduction [25]. The loss in reducibilities can be probably attributed to a non-reducible (at temperatures <800 °C) "Co-titanate" species

Table 1
Surface areas, reducibilities and reducibility loss after reduction of samples after various pretreatments

Samples	Surface area ($m^2\ g^{-1}$)	Reducibility during TPR at 35–800 °C (%)[a,b]	Reducibility loss after reduction (%)[c]
T1	70	0	–
T2	49	0	–
Co/T1 (C)	52	92	n/a
Co/T2 (C)	37	78	n/a
Co/T1 (RW0)	49	70	24
Co/T2 (RW0)	37	74	5
Co/T1 (RW5)	46	68	26
Co/T2 (RW5)	37	72	8
Co/T1 (RW10)	46	64	30
Co/T2 (RW10)	36	68	13

[a] The reduced samples were recalcined at the original calcination conditions prior to performing TPR. The reducibility was calculated based on the area below TPR curve, which was related to the amounts of H_2 consumed during TPR (calibrated using Ag_2O).
[b] Measurement error is ±5%.
[c] Reducibility loss (%) after reduction was calculated from [(reducibility of calcined sample − reducibility of reduced sample) × 100]/reducibility of calcined sample.

formed during standard reduction [25]. However, when considering the reducibility loss of the reduced samples without hydrothermal treatment (RW0 samples), it was found that the reducibility loss after reduction for Co/T2-RW0 sample was only 5%, whereas the 24% reducibility loss after reduction was observed for Co/T1-RW0 sample. A degree of reducibility loss also increased with the amounts of water vapor added during reduction for both T1 and T2 supports. In order to illustrate the reducibility loss upon the hydrothermal treatment during standard reduction for both T1 and T2 supports, Fig. 4 is also present. This is to provide a better idea how the presence of rutile phase leads to an increase in stability of the catalysts upon reduction and hydrothermal treatments in term of the reducibility loss after reduction under various conditions.

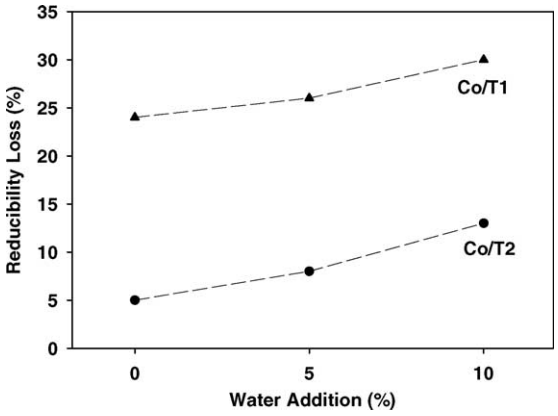

Fig. 4. A comparison of reducibility loss (%) during reduction with hydrothermal treatment for Co/T1 and Co/T2 catalyst samples.

3.2. Catalytic properties

In order to determine the effect of crystalline phases of titania on the catalytic properties of Co/TiO_2, CO hydrogenation was also conducted in a fixed-bed flow reactor under differential conditions. Results obtained from the reaction study are shown in Table 2. It was found that both initial and steady-state rates increased significantly upon the presence of rutile phase in titania as seen for catalysts on the T2 support. However, the increased activities for catalysts on the T1 support strongly depended on the pretreatment conditions used. For catalysts on the T1 support, it was shown that decreases in both initial and steady-state activities were proportional to the amounts of water vapors added during standard reduction. It should be also noted that decreases in activities were also related to the loss in reducibilities after standard reduction as well. Considering both initial and steady-state rates for catalysts on the T2 support, the phenomenon was essentially different from those for the T1 support. It was found that activities for catalysts on the T2 support exhibited much higher activities than those on the T1 support, especially, at the same hydrothermal treatment conditions. Moreover, the

Table 2
Reaction study during CO hydrogenation of catalyst samples pretreated under various conditions

Samples	CO conversion (%)[a]		Rate ($\times 10^2$ $gCH_2\ g_{cat}\ h^{-1}$)[b]		CH_4 selectivity (%)	
	Initial[c]	SS[d]	Initial	SS	Initial	SS
Co/T1 (C)	3.7	2.1	1.4	0.8	71	68
Co/T2 (C)	67.4	54.9	25	21	94	96
Co/T1 (RW0)	1.5	0.7	0.6	0.3	68	65
Co/T2 (RW0)	60.8	53.1	23	20	94	94
Co/T1 (RW5)	0.8	0.5	0.3	0.2	71	70
Co/T2 (RW5)	60.6	52.8	23	20	98	98
Co/T1 (RW10)	0.3	0.1	0.1	0.03	73	69
Co/T2 (RW10)	60.2	52.6	23	19	95	96

[a] CO hydrogenation was carried out at 220 °C, 1 atm and $H_2/CO/He = 20/2/8$ cc min^{-1}.
[b] Error ±5%. Rate of $-CH_2-$ formed as same as moles of CO converted represented the repeating unit of all hydrocarbon chains in product stream.
[c] After 5 min of reaction.
[d] After 5 h of reaction.

Table 3
Influence of surface area of TiO_2 on catalytic properties of supported cobalt catalysts during CO hydrogenation

Samples	Surface area ($m^2\ g^{-1}$)	CO conversion (%)[a]		Rate ($10^2\ gCH_2\ g_{cat}\ h^{-1}$)[b]	
		Initial[c]	SS[d]	Initial	SS
Co/T1 (C)	70	3.7	2.1	1.4	0.8
Co/T3 (C)[e]	145	42.7	9.4	16	4
Co/T4 (C)[f]	170	59.6	12.2	22	4
Co/T2 (C)	49	67.4	54.9	25	21

[a] CO hydrogenation was carried out at 220 °C, 1 atm and $H_2/CO/He = 20/2/8$ cc min^{-1}.
[b] Error ±5%.
[c] After 5 min of reaction.
[d] After 5 h of reaction.
[e] T3 is TiO_2 (pure anatase) which has surface area of 145 $m^2\ g^{-1}$.
[f] T4 is TiO_2 (pure anatase) which has surface area of 170 $m^2\ g^{-1}$.

initial activities of catalysts on the T2 support exhibited a lesser degree of decreased rates until they reached the steady-state rates compared to those on the T1 support. In addition, for catalysts on the T2 support, both initial and steady-state rates showed consistency in rates regardless of the pretreatment conditions used indicating high stability of catalysts. This is suggested that the hydrothermal treatment conditions used have no effect on the catalytic activities during CO hydrogenation of catalysts on the T2 support. This can be explained by the increased stability of T2 support due to the presence of rutile phase in titania resulting in an inhibition of Co-support compound formation (Co-SCF) [19,20] in the titania support [25].

Since the surface areas of the T1 (70 $m^2\ g^{-1}$) and T2 (49 $m^2\ g^{-1}$) supports were slightly different, one might think that a change in surface areas of the supports probably has the effect on rates as well. In order to elucidate this doubt, reaction study was also conducted using titania supports (anatase form only) with various surface areas. Results obtained from the reaction study are shown in Table 3. It was found that basically, both initial and steady-state activities increased with increasing surface areas from 70 to 170 $m^2\ g^{-1}$ for catalysts on pure anatase titania. This should be due to higher Co dispersion in larger surface areas of supports leading to an increase in the number of reduced surface Co metal atoms available for catalyzing the reaction. Thus, if one considered the dependence of rates based on the surface areas solely, catalysts on the T2 support, which had smaller surface areas would result in lower activities due to a decreased surface area. However, it is not true for what we have found in this present study. Essentially, even though the surface area of the T2 support was only 49 $m^2\ g^{-1}$, which was smaller than that for the pure anatase titania, activities of catalysts on the T2 support were still exceptional high with the presence of rutile phase in titania. This indicated that the presence of rutile phase in titania can result in an enhancement of catalytic activities of Co/TiO_2 catalyst during CO hydrogenation. Increases in activities were probably due to: (i) high stability to the hydrothermal treatment of the support used; and (ii) the presence of a higher number of reduced Co metal atoms resulted from the lesser amounts of Co-SCF.

Considering the selectivity of products during methanation, which is also shown in Table 2. It was found that catalysts on the T2 support exhibited higher selectivity to methane compared to those on the T1 support. This was suggested that catalysts on the T1 support produced more long chain hydrocarbons than those on the T2 support. This indicated that the presence of rutile phase on titania probably resulted in a lesser amounts of long chain hydrocarbons. In general, it has been known that catalytic activities of supported Co catalyst depend only on the number of surface reduced cobalt atoms available for catalyzing the reaction. Mostly, changes in catalytic activities do not alter the selectivity of products since only the number of active sites change, but the nature of active sites would be the same. However, in this case, we found a slight change in product selectivity. This indicated that the presence of rutile phase in titania affected not only on activities of Co/TiO_2 catalysts, but perhaps also on the selectivity of products as well. In order to give the best answer for how the presence of rutile phase affects the selectivity of products during CO hydrogenation, a rigorous study should be further investigated in more details. It is recommended that techniques such as steady-state isotropic transient kinetic analysis (SSITKA) or other surface analysis techniques must be applied in order to provide more details on the surface intermediates. Thus, this is not the main focus of our present study at this time. Besides, influences of rutile phase in titania on product distributions, an investigation of how the mole ratios of rutile per anatase phase affect the catalytic properties will be our main focus in the near future.

4. Conclusions

The present study has shown the dependence of crystalline phases in titania on the catalytic properties during CO hydrogenation of Co/TiO_2 catalysts. The presence of rutile phase (19 mol%) in titania resulted in significant increases in the catalytic activities during CO hydrogenation. This is mostly due to an increase in stability of the titania support with the presence of rutile phase. It was found that the presence of rutile phase enhanced the stability of the titania support and

also catalysts themselves leading to lesser degrees of a loss in reducibility after hydrothermal treatments during reduction of catalysts. It was proposed that the presence of rutile phase in titania stabilized the catalysts probably due to two reasons: (i) block the formation of Co species strongly interacted with the titania support or Co-SCF; and (ii) inhibition of the impact of water vapor produced during reduction.

Acknowledgements

We gratefully acknowledge the financial support by the National Research Council of Thailand (NRCT), the Thailand Research Fund (TRF) and Thailand-Japan Transfer Technology Project (TJTTP-JBIC). We would like to thank Prof. James G. Goodwin, Jr. at Clemson University for initiating this kind of project. We would like to extend our thanks to the National Metal and Materials Technology Center (MTECH) for Raman spectroscopy analysis.

References

[1] H.P. Wither Jr., K.F. Eliezer, J.W. Mechell, Ind. Eng. Chem. Res. 29 (1990) 1807.
[2] E. Iglesia, Appl. Catal. A 161 (1997) 59.
[3] R.C. Brady, R.J. Pettie, J. Am. Chem. Soc. 103 (1981) 1287.
[4] A. Martinez, C. Lopez, F. Marquez, I. Duaz, J. Catal. 220 (2003) 486.
[5] J. Panpranot, J.G. Goodwin Jr., A. Sayari, Catal. Today 77 (2002) 269.
[6] J. Panpranot, J.G. Goodwin Jr., A. Sayari, J. Catal. 211 (2002) 530.
[7] S.L. Sun, I. Isubaki, K. Fujimoto, Appl. Catal. A 202 (2000) 121.
[8] S. Ali, B. Chen, J.G. Goodwin Jr., J. Catal. 157 (1995) 35.
[9] B. Jongsomjit, J. Panpranot, J.G. Goodwin Jr., J. Catal. 215 (2003) 66.
[10] T. Das, G. Jacobs, P.M. Patterson, W.A. Conner, J.L. Li, B.H. Davis, Fuel 82 (2003) 805.
[11] G. Jacobs, P.M. Patterson, Y.Q. Zhang, T. Das, J.L. Li, B.H. Davis, Appl. Catal. A 233 (2002) 215.
[12] M. Rothaemel, K.F. Hanssen, E.A. Blekkan, D. Schanke, A. Holmen, Catal. Today 38 (1997) 79.
[13] V. Ragaini, R. Carli, C.L. Bianchi, D. Lorenzetti, G. Vergani, Appl. Catal. A 139 (1996) 17.
[14] V. Ragaini, R. Carli, C.L. Bianchi, D. Lorenzetti, G. Predieri, P. Moggi, Appl. Catal. A 139 (1996) 31.
[15] J.L. Li, G. Jacobs, T. Das, B.H. Davis, Appl. Catal. A 233 (2002) 255.
[16] G. Jacobs, T. Das, Y.Q. Zhang, J.L. Li, G. Racoillet, B.H. Davis, Appl. Catal. A 233 (2002) 263.
[17] J.L. Li, L.G. Xu, R. Keogh, B.H. Davis, Catal. Lett. 70 (2000) 127.
[18] X.H. Li, K. Asami, M.F. Luo, K. Michiki, N. Tsubaki, K. Fujimoto, Catal. Today 84 (2003) 59.
[19] B. Jongsomjit, J. Panpranot, J.G. Goodwin Jr., J. Catal. 204 (2001) 98.
[20] B. Jongsomjit, J.G. Goodwin Jr., Catal. Today 77 (2002) 191.
[21] A. Kogelbaue, J.C. Weber, J.G. Goodwin Jr., Catal. Lett. 34 (1995) 269.
[22] Y. Zhang, D. Wei, S. Hammache, J.G. Goodwin Jr., J. Catal. 188 (1999) 281.
[23] D. Schanke, S. Vada, E.A. Blekkan, A. Hilmen, A. Hoff, A. Holmen, J. Catal. 156 (1995) 85.
[24] B.A. Sexton, A.E. Hughes, T.W. Turney, J. Catal. 97 (1986) 390.
[25] B. Jongsomjit, C. Sakdamnuson, J.G. Goodwin Jr., P. Praserthdam, Catal. Lett. 94 (2004) 209.

LLDPE/nano-silica composites synthesized via *in situ* polymerization of ethylene/1-hexene with MAO/metallocene catalyst

BUNJERD JONGSOMJIT*, EKKRACHAN CHAICHANA, PIYASAN PRASERTHDAM
Center of Excellence on Catalysis and Catalytic Reaction Engineering, Department of Chemical Engineering, Faculty of Engineering, Chulalongkorn University, Bangkok 10330, Thailand
E-mail: bunjerd.j@chula.ac.th

It is known that the copolymerization of ethylene with higher 1-olefins is a commercial importance for productions of elastomer and linear low-density polyethylene (LLDPE). LLDPE (density 0.920 to 0.940) is one of the most widely used polyolefins in many applications, especially, for plastic films. However, in some cases, the use of polyolefins or LLDPE is limited by their drawbacks such as low mechanical strength, low thermal resistance, poor optical properties and so on. Thus, in order to improve the specific properties of these polymers, some additives need to be blended with them.

It has been reported that blending polymer with inorganic materials is considered as a powerful method to produce new materials called polymer composites or filled polymers. However, due to the significant development in nano-technologies in the recent years, nano-inorganic materials such as SiO_2, Al_2O_3 and TiO_2 have brought much attention to this research field. Therefore, the polymer composites filled with nano-inorganic materials are well recognized as polymer nano-composites. Essentially, addition of the nano-materials into polymers may lead to overcome the drawbacks and produce new materials, which are considered to be robust. Basically, there are three methods used to produce the filled polymer; (i) melt mixing, (ii) solution blending, and (iii) *in situ* polymerization. Due to the direct synthesis via polymerization along with the presence of nano-materials, the *in situ* polymerization is perhaps considered to be the most powerful techniques to produce polymer nano-composites with good dispersion of the nano-particles into polymer matrix. Although, many authors [1–6] have studied LLDPE composites only synthesized via melt mixing and solution blending, no further reports have been done on synthesizing polymer nano-composites via the *in situ* polymerization with metallocene catalysts.

In the present study, LLDPE/nano-SiO_2 composites synthesized via the *in situ* polymerization with MAO/metallocene catalyst was investigated for the first time. The nano-SiO_2 and nano-SiO_2 doped Al_2O_3 filled materials were synthesized using sol-gel method [7] to obtain the nano-SiO_2 with particle size of ca. 50 nm. The amounts of nano-materials filled were also varied. Yields, activities, and polymer morphologies were discussed.

The preparation of LLDPE/nano-composites via *in situ* polymerization was performed as follows; all chemicals [nano-SiO_2, nanoSiO_2 doped Al_2O_3, toluene, rac-ethylenebis (indenyl) zirconium dichloride [$Et(Ind)_2ZrCl_2$], methylaluminoxane (MAO), trimethylaluminum (TMA) and 1-hexene] were manipulated under an inert atmosphere using a vacuum glove box and/or Schelenk techniques. The nano-materials were heated under vacuum at 400 °C for 6 hr prior to impregnation with MAO. In order to impregnate MAO onto the nano-materials, the method was described as follows. One gram of the nano-materials was reacted with the desired amount of MAO at room temperature and stirred for 30 min. The solvent was then removed from the mixture. About 20 ml of toluene was added into the obtained precipitate, the mixture was stirred for 5 min, and then the solvent was removed. This procedure was done for five times to ensure the removal of impurities. Then, the solid part was dried under vacuum at room temperature to obtain white powder of nano-materials/ MAO.

Polymerization was conducted upon the methods as follows. The ethylene/1-hexene copolymerization reaction was carried out in a 100-ml semi-batch stainless steel autoclave reactor equipped with a magnetic stirrer. At first, 0.1, 0.2, and 0.3 g of the nano-materials/MAO ($[Al]_{MAO}/[Zr]$ = 1135, 2270, and 3405) and 0.018 mole of 1-hexene along with toluene (to make the total

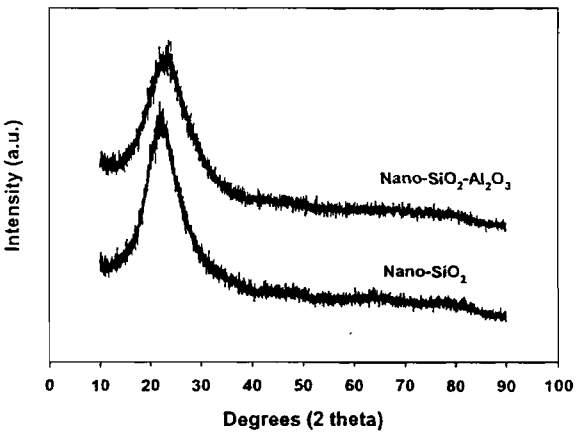

Figure 1 XRD patterns of nano-SiO_2 and nano-SiO_2-Al_2O_3.

*Author to whom all correspondence should be addressed.

0022–2461

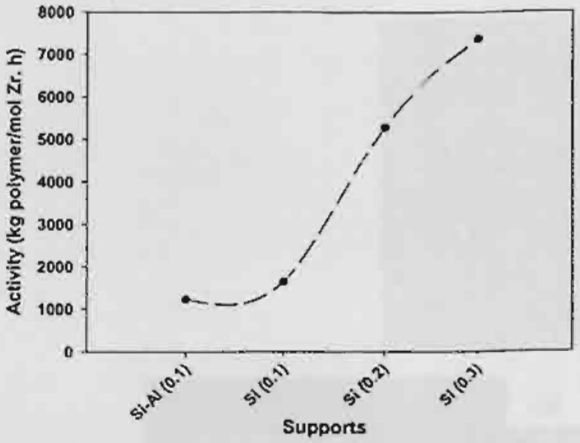

Figure 2 Activity profile with various amounts of support used.

volume of 30 ml) were put into the reactor. The desired amount of $Et(Ind)_2ZrCl_2$ (5×10^{-5} M) and TMA ($[Al]_{TMA}/[Zr] = 2500$) was mixed and stirred for 5-min aging at room temperature, separately, and then was injected into the reactor. The reactor was frozen in liquid nitrogen to stop reaction for 15 min and then the reactor was evacuated to remove argon. The reactor was heated up to polymerization temperature (70 °C). To start reaction, 0.018 mole of ethylene was fed into the reactor containing the comonomer and catalyst mixtures. After all ethylene was consumed, the reaction was terminated by addition of acidic methanol (0.1% HCl in methanol) and stirred for 30 min. After filtration, the obtained copolymer (white powder) was washed with methanol and dried at room temperature. The LLDPE/nano-SiO_2 composites obtained were characterized using scanning electron microscopy (SEM) and energy dispersive X-ray spectroscopy (EDX) to study morphologies and elemental distribution, respectively.

TABLE I Activity and yield of LLDPE/nano-composites via *in situ* polymerization with metallocene catalyst

Nano-filled	Amounts/Run (g)	Yield (g)	Time (s)	Activity (kg pol./mol. Zr.h)
SiO_2–Al_2O_3	0.1	0.2006	450	1234
SiO_2	0.1	0.2147	360	1652
SiO_2	0.2	0.6070	318	5288
SiO_2	0.3	0.8382	315	7369

XRD patterns of nano-SiO_2 and nano-SiO_2-Al_2O_3 are shown in Fig. 1. It was found that XRD patterns for both materials exhibited similar patterns assigning to amorphous silica. No XRD peaks of Al_2O_3 were detected indicating highly dispersed forms of it. After impregnation of MAO onto the nano-particles, copolymerization of ethylene/1-hexene was performed with various conditions based on changing types and/or amounts of the nano-particles used. Activities and yields of LLDPE/nono-composites are shown in Table I. It was observed that activities and yields dramatically increased with increasing the amounts of SiO_2 particles used due to increased MAO as a cocatalyst. However, at the same amount (0.1 g) of particles, the SiO_2-Al_2O_3 exhibited the lowest yield and activity of any other samples. A comparison of activities is also shown in Fig. 2. It should be noted that activities of LLDPE/nano-SiO_2 composites obtained in this present study were much lower (about three times) compared to the LLDPE/micron-SiO_2 composite as reported by our group [8]. This was probably due to more steric hindrance arising from the nano-particles. Morphologes of LLDPE/nano composites are shown in Fig. 3.

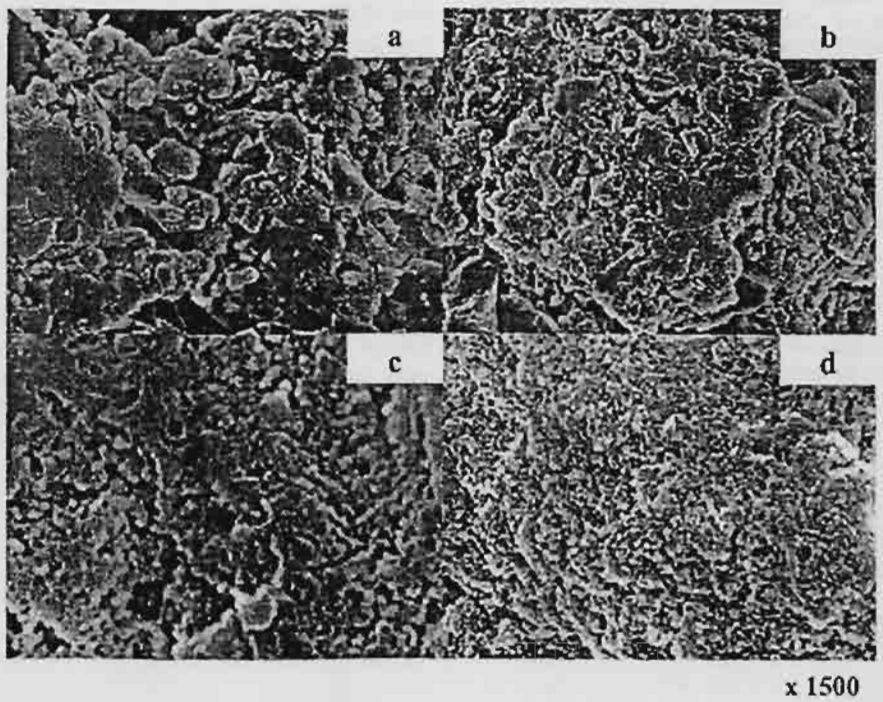

Figure 3 Morphologies of LLDPE/nano composites with: (a) SiO_2–Al_2O_3 (0.1 g), (b) SiO_2 (0.1 g), (c) SiO_2 (0.2 g), and (d) SiO_2 (0.3 g).

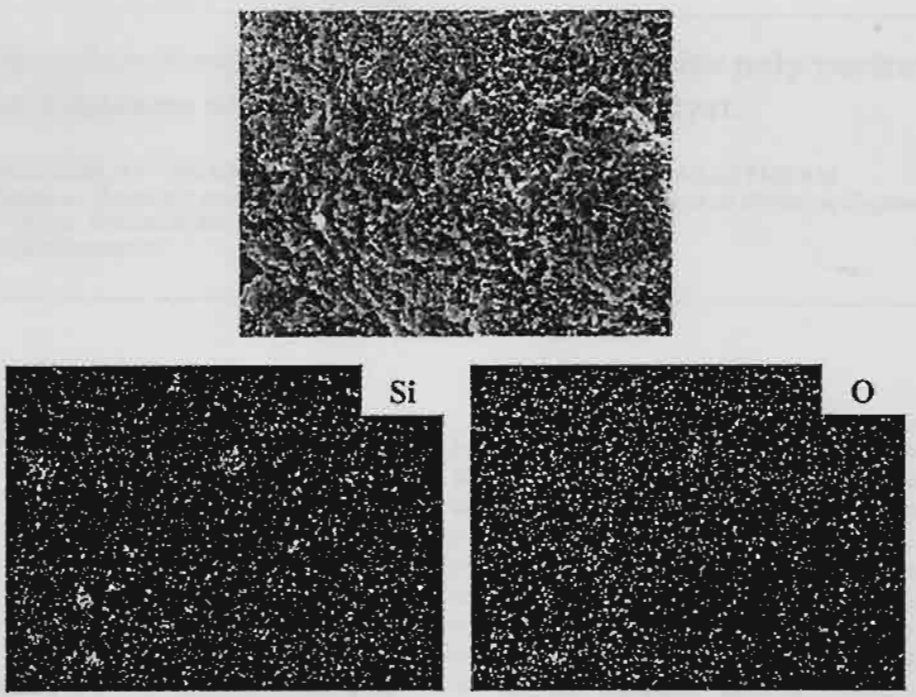

Figure 4 EDX mapping of LLDPE/nano-SiO_2 composite with SiO_2 (0.3 g) indicating distribution of Si and O.

It can be observed that with using SiO_2-Al_2O_3 (0.1 g), SiO_2 (0.1 g), and SiO_2 (0.2 g), morphologies [Fig. 3a–c] were found to be similar indicating only the polymer texture as seen in ref. [8]. However, with increasing the amount of nano-SiO_2 to 0.3 g, the morphology as shown in Fig. 3d was significantly changed indicating better combination between the silica and polymer textures. This was suggested that the LLDPE/nano-SiO_2 composite can be obtained at a certain amount of the nano-SiO_2 particles used. In order to identify the distribution of SiO_2 particles in the polymer matrix, EDX mapping was performed on the distribution of Si and O elements as shown in Fig. 4. It can be observed that Si and O elements exhibited good distribution all over the polymer matrix indicating good dispersion of nano-SiO_2 particles.

In summary, LLDPE/nano-SiO_2 composites can be obtained via the *in situ* polymerization with MAO/metallocene catalyst. It was found that silica particles were well dispersed in the polymer matrix at some certain amounts of them. However, activities and yields of polymerization were apparently low probably due to more steric hindrance arising from the nano-particles. Thus, polymerization conditions, catalysts used, and types of nano-particles need to be further investigated in order to increase productivity.

Acknowledgments

The authors would like to thank the Thailand Research Fund (TRF), National Research Council of Thailand (NRCT) and Thailand-Japan Transfer Technology Project (TJTTP-JBIC) for the financial support of this work. The authors would also like to thanks Prof. Takeshi Shiono at Hiroshima University, Japan, for his kind adviee throughout this project.

References

1. C. J. R. VERBEEK, *Mater. Lett.* 56 (2002) 226.
2. R. NAWANG, I. D. DANJAJI, U. S. ISHIAKU, H. ISMAIL and Z. A. MOHD ISHAK, *Polym. Testing.* 20 (2001) 167.
3. Y. HAUNG, S. JIANG, L. WU and Y. HUA, *ibid.* 23 (2004) 9.
4. Y. Q. HUANG, Y. Q. ZHANG and Y. Q. HUA, *J. Mater. Sci. Lett.* 22 (2003) 997.
5. I. D. DANJAJI, R. NAWANG, U. S. ISHIAKU, H. ISMAIL and Z. A. MOHD ISHAK, *Polym. Testing* 21 (2002) 75.
6. C. J. R. VERBEEK, *Mater. Lett.* 52 (2002) 453.
7. M. BUCKLEY and M. GREENBLATT, *J. Chem. Edu.* 71 (1994) 599.
8. B. JONGSOMJIT, P. PRASERTHDAM and P. KAEWKRAJANG, *Mater. Chem. Phys.* 86 (2004) 243.

Received 20 September
and accepted 7 October 2004